Giuseppe Colella, Allan D. Mackie, James P. Larentzos, John K. Brennan, Martin Lísal and Josep Bonet Avalos*

Generalized energy-conserving dissipative particle dynamics with mass transfer: coupling between energy and mass exchange

Abstract: The complete description of energy and material transport within the Generalized energy-conserving dissipative particle dynamics with mass transfer (GenDPDE-M) methodology is presented. In particular, the dynamic coupling between mass and energy is incorporated into the GenDPDE-M, which was previously introduced with dynamically decoupled fluxes (J. Bonet Avalos et al., *J. Chem. Theory Comput.*, 18 (12): 7639–7652, 2022). From a theoretical perspective, we have derived the appropriate Fluctuation-Dissipation theorems along with Onsager's reciprocal relations, suitable for mesoscale models featuring this coupling. Equilibrium and nonequilibrium simulations are performed to demonstrate the internal thermodynamic consistency of the method, as well as the ability to capture the Ludwig–Soret effect, and tune its strength through the mesoscopic parameters. In view of the completeness of the presented approach, GenDPDE-M is the most general Lagrangian method to deal with complex fluids and systems at the mesoscale, where thermal agitation is relevant.

Keywords: dissipative particle dynamics; nonequilibrium thermodynamics; coupled energy-mass transfer; thermodiffusion

1 Introduction

The macroscopic behavior and properties of complex systems such as biological matter, composite materials or complex fluids, depend on the dynamics of phenomena occurring at the micro- and mesoscale. For such systems, the coupling between energy and mass transport is important for the understanding of several physicochemical scenarios, ranging from molecular motors to heterogeneous catalysis, with many important applications, e.g., in most chemical engineering processes. While atomistic modeling and simulation is a valuable tool, the computational cost of its application to such complex systems, whose characteristic temporal and spatial breadths are typically large compared to molecular dimensions, is often prohibitive. Coarse-grain (CG) modeling has become a vital alternative in cases where atomistic approaches are limiting or impractical. Among the wide variety of CG methods developed over the last decades, Dissipative Particle Dynamics (DPD) [1] has become a popular

*Corresponding author: Josep Bonet Avalos, Departament d'Enginyeria Química, ETSEQ, Universitat Rovira i Virgili, Tarragona, 43007, Spain, E-mail: josep.bonet@urv.cat. https://orcid.org/0000-0002-7339-9564
Giuseppe Colella and **Allan D. Mackie**, Departament d'Enginyeria Química, ETSEQ, Universitat Rovira i Virgili, Tarragona, 43007, Spain. https://orcid.org/0000-0002-6743-161X (G. Colella), https://orcid.org/0000-0002-1819-7820 (A.D. Mackie)
James P. Larentzos and **John K. Brennan**, U.S. Army Combat Capabilities Development Command (DEVCOM) Army Research Laboratory, Aberdeen Proving Ground, MD, 21005, USA. https://orcid.org/0000-0002-9873-4349 (J. P. Larentzos). https://orcid.org/0000-0001-9573-5082 (J. K. Brennan)
Martin Lísal, Research Group of Molecular and Mesoscopic Modelling, The Czech Academy of Sciences, Institute of Chemical Process Fundamentals, Prague, Czech Republic; and Department of Physics, Faculty of Science, Jan Evangelista Purkyně University in Ústí nad Labem, Ústí nad Labem, 40096, Czech Republic. https://orcid.org/0000-0001-8005-7143

tool. Standard DPD is a Lagrangian, Galilean-invariant method whose dynamics conserves the total momentum and number of particles. As a consequence, the associated fields satisfy the corresponding hydrodynamic equations in the hydrodynamic limit [2], namely, Navier–Stokes and continuity equations [3]. In the standard DPD approach, the total force acting on a CG particle takes into account conservative as well as dissipative forces. The dissipation enters into the description through the CGing, due to the coupling between the resolved and CG degrees of freedom. Wherever dissipation occurs, implicitly there is a random contribution due to the thermal agitation of the non-resolved degrees of freedom [2]. In the DPD method, these contributions are added in the form of Langevin-like random forces between particles, which still preserve the Galilean invariance of the model. The dissipative friction force depends on both the positions and linearly on the velocity difference between the particles, through a coefficient that determines the strength of the force. The random contribution, on the other hand, is characterized by a Gaussian distribution and an amplitude that is related to the strength of the friction force through the corresponding Fluctuation-Dissipation (FD) theorem. In standard DPD method, the intensity of the random force depends on the system temperature T as a parameter [4]. Therefore, DPD is by construction isothermal and as a consequence heat flow cannot be modeled. An extension of the original DPD method was developed afterwards to include energy conservation, referred to as DPD with Energy Conservation (DPDE) [5], [6]. In DPDE, particles carry internal energy, stored into the CG degrees of freedom, and exhibit a *particle temperature* involved in the interparticle heat exchange. Since their development, both DPD and DPDE have been increasingly applied in different research areas [7]–[10]. Recently, the Generalized Energy-Conserving DPD (GenDPDE) method [11], [12] has been proposed as a further extension of DPDE. The fundamental idea behind GenDPDE is the introduction of a particle fluctuating thermodynamics, which allows for a consistent definition of many-body forces that can depend on the particle temperature and particle density, unlike previous many-body DPD models in which the forces depend only on the local density [13]–[20], or even parametrically on the system temperature [21]. More specifically, within the GenDPDE framework the force exerted by each mesoparticle can be related to its internal pressure, which depends on the particle volume and temperature through a particle Equation of State (EoS). In this way, the GenDPDE method permits the definition of temperature- and density-dependent forces, which are relevant for modeling non-equilibrium phenomena occurring in systems undergoing, e.g., chemical reactions [22] or shock compressions [23].

The concept of a fluctuating particle thermodynamics readily allowed for an extension of the GenDPDE framework to also include chemical composition into the description of the particle thermodynamic state. This extension is referred to as GenDPDE-M [24], [25]. Analogous to the heat flux in GenDPDE, in the new framework matter can be exchanged with neighboring mesoparticles through diffusive fluxes. However, GenDPDE-M in its first formulation (see the aforementioned references) disregarded any dynamic coupling between energy and material transport, which is in reality present in many relevant physical scenarios. Therefore, the introduction of the dynamic coupling between energy and mass fluxes presented in this work is a critical extension of GenDPDE-M.

In this article, we develop the theoretical framework to account for the coupling between mass and energy transport at the mesoscale. The outcome of our work is, therefore, a GenDPDE-M method that is complete and allows general, complex cases, involving momentum, energy and material transports, to be addressed in a unified way. Thus, within the complete GenDPDE-M method, phenomena such as the Ludwig–Soret effect can be properly modeled.

The manuscript is organized as follows. In Section 2, we review the theoretical framework based on the definition of the heat and diffusive fluxes along the lines of classical Onsager's non-equilibrium thermodynamics [26], formulated at the mesoscale, where thermal agitation is relevant. We derive Langevin equations for the coupled energy and mass transfers to account for the thermal fluctuations. We highlight the key role of Detailed Balance (DB) in consistently formulating the fluctuating dynamics of complex CG systems. We show that DB not only sets the amplitude of the random contributions through FD relations, but also imposes the validity of Onsager's reciprocal relations (ORR) at the mesoscopic level. We then introduce the van der Waals (vdW) particle thermodynamic model as a case study, which is used in both equilibrium and non-equilibrium simulations. In Section 3, we provide the computational details regarding our GenDPDE-M simulations. In Section 4, we present data obtained from equilibrium and non-equilibrium simulations. From these simulations, we show the

consistency of the fluctuating local thermodynamic description, when coupling between mass and energy is present. Moreover, non-equilibrium simulations results are shown in which the dependency of the Ludwig–Soret effect on the strength of the mesoscopic coupling is discussed, along with the impact of the latter on the thermal conductivity of the system. Finally, Section 5 provides conclusions and future outlooks regarding GenDPDE-M.

2 Theoretical framework

In the general GenDPDE-M framework [24], [25], mesoparticles are regarded as property carriers whose state and dynamics are ultimately inherited from an existing underlying physical system. The latter can be regarded as being described by a classical Hamiltonian, with time-reversible trajectories, which ensures that an equilibrium probability distribution function exists and that DB is satisfied. The mesoscopic state variables are then a collection of *surviving* variables resulting from the CG process. Due to the elimination of internal degrees of freedom (*non-surviving* variables), the mesoscopic state variables can then be treated in a manner analogous to macroscopic Thermodynamics. For a simple multicomponent system, these surviving variables are the mesoparticle mass, m_i, position, $\mathbf{r}_i$, momentum, $\mathbf{p}_i$, internal energy, u_i, number density, n_i (representative of the mesoparticle volume), and chemical composition. The dependence of the particle state on the chemical composition was introduced in the formulation of GenDPDE-M to incorporate material exchange into the GenDPDE framework [11], [12]. To describe composition, let us assume that the underlying physical system contains a number N_s of different chemical species, each denoted by α and having a molecular mass $\bar{m}_\alpha$. Due to the CG process, a given number of these particles can be found within mesoparticle i at a given instant of time. This number is denoted by $\mathcal{N}_i^\alpha$. These $\mathcal{N}_i^\alpha$ physical particles are thus *embedded* into mesoparticle i and hence contribute to its mass with $m_i^\alpha = \mathcal{N}_i^\alpha \bar{m}_\alpha$. Therefore, the composition of mesoparticle i is specified by the set of aggregate masses of the embedded species, i.e., by the set $\left\{ m_i^\alpha \right\}_{\alpha=1}^{N_s}$.

It is very important to realize that a given extensive property should be specified for each mesoparticle, to characterize its size. Without loss of generality, we fix the total mesoparticle mass $m_i = \sum_{\alpha=1}^{N_s} m_i^\alpha$ as the size characterization. This choice is compatible with the mesoparticle velocity being an estimator of the so-called *baricentric velocity* [26], [27] (which is used in the Navier–Stokes equation and has a central role in fluid mechanics), and has the added benefit of decoupling the mechanical dynamics of the system from the particle composition. Therefore, the diffusive fluxes are defined as material fluxes relative to the baricentric motion of the mesoparticles, so that not all of them are independent, since

$$\mathrm{d}m_i = \sum_{\alpha=1}^{N_s} \mathrm{d}m_i^\alpha = 0 \tag{1}$$

due to the constant mass constraint. Here, $\mathrm{d}m_i^\alpha$ represents an arbitrary variation of the mass of species α. Thus, in the GenDPDE-M framework, only $N_s - 1$ masses of the embedded species are treated as independent variables. Other choices, such as fixing the total molar number, are also possible, in which case $\mathrm{d}\mathcal{N}_i = \sum_{\alpha=1}^{N_s} \mathrm{d}\mathcal{N}_i^\alpha = 0$. However, it is well known that the physical dynamic processes related to advection and diffusion are independent of these choices [26], [27].

In the following, we formulate heat and diffusive fluxes with coupling between them, which go beyond the initial approach presented in Refs. [24], [25]. We start by introducing, in Section 2.1, the concept of the particle fluctuating thermodynamics while the particles are kept at rest, for simplicity. We further outline the central object of the mesoscale thermodynamic description, i.e., the probability distributions for the state variables. In Section 2.2, we introduce the heat and diffusive fluxes, using Onsager's formulation of non-equilibrium processes at the mesoscopic level [26], [28], since particles at rest can still exchange energy and mass due to these fluxes. We then provide explicit expressions for the general relations between the heat and diffusive fluxes with the corresponding thermodynamic forces, together with the associated random contributions, in Section 2.3. Finally, we derive the complete Equations-of-Motion (EoM) for the system of moving particles, which exchange energy

and matter (Section 2.4). For completeness, in Section 2.5 we provide an example of a thermodynamic model for the mesoparticles, which is used in the simulations.

2.1 Probability distribution and intensive variables

For simplicity and clarity, but without loss of generality, let us consider mesoparticles with their positions fixed in space. Moreover, we restrain the discussion to binary mixtures ($N_s = 2$). Although the generalization to multicomponent systems is straightforward, it requires quite a lengthy algebraic treatment [27].

The state of a *static* mesoparticle is defined by specifying its energetic content u_i and the mass of the A-component m_i^A. Here, we can ignore the density n_i as a state variable, since the latter enters the thermodynamic description only parametrically for static particles, along with the constant particle mass m_i. Due to the mass constraint Eq. (1), the amount of the second component B is simply given by

$$m_i^B = m_i - m_i^A > 0 \tag{2}$$

Following the analysis in Refs. [11], [12], the canonical equilibrium probability distribution for a system of N static mesoparticles with an embedded binary mixture is given by

$$P_{\mathrm{eq}}(\tilde{\Gamma}) = P_{\mathrm{eq}}(\{u_i\}, \{m_i^A\}) \propto e^{-\sum\limits_{i=1}^{N} [u_i - T\tilde{s}_i(u_i, m_i^A)]/(k_B T)} \tag{3}$$

where $\tilde{\Gamma} \equiv (\{u_i\}, \{m_i^A\})$, k_B is the Boltzmann constant, T is the reservoir temperature, and $\tilde{s}_i$ is the so-called *bare* particle entropy, which is a function of u_i and m_i^A [29]. From a physical point of view, the bare entropy is related to the density of microscopic states g for the CG variables within the mesoparticle for given u_i and m_i^A [11], i.e.,

$$\tilde{s}_i = k_B \ln g(u_i, m_i^A) \tag{4}$$

In Eq. (3) we have explicitly assumed that the independent variables are the particles energies, u_i, and the mass of species A, m_i^A. According to Refs. [11], [12], by analogy with macroscopic thermodynamics, without loss of generality we can write,

$$d\tilde{s}_i = \frac{\partial \tilde{s}_i}{\partial u_i}\bigg|_{m_i^A, m_i^B} du_i + \frac{\partial \tilde{s}_i}{\partial m_i^A}\bigg|_{u_i, m_i^B} dm_i^A + \frac{\partial \tilde{s}_i}{\partial m_i^B}\bigg|_{u_i, m_i^A} dm_i^B$$

$$\equiv \frac{1}{\tilde{\theta}_i} du_i - \frac{\tilde{\mu}_i^A}{\tilde{\theta}_i} dm_i^A - \frac{\tilde{\mu}_i^B}{\tilde{\theta}_i} dm_i^B \tag{5}$$

which is a definition of the bare intensive variables,

$$\frac{\partial \tilde{s}_i}{\partial u_i}\bigg|_{m_i^A, m_i^B} \equiv \frac{1}{\tilde{\theta}_i} \tag{6}$$

$$\frac{\partial \tilde{s}_i}{\partial m_i^A}\bigg|_{u_i, m_i^B} \equiv \frac{\tilde{\mu}_i^A}{\tilde{\theta}_i} \tag{7}$$

$$\frac{\partial \tilde{s}_i}{\partial m_i^B}\bigg|_{u_i, m_i^A} \equiv \frac{\tilde{\mu}_i^B}{\tilde{\theta}_i} \tag{8}$$

where $\tilde{\theta}_i$ is the bare particle temperature and $\tilde{\mu}_i^A$, and $\tilde{\mu}_i^B$ are the respective species bare chemical potentials. Then, using Eq. (1) we can eliminate the dependent variable m_i^B in Eq. (5), and introduce the exchange chemical potential $\bar{\tilde{\mu}}_i \equiv \tilde{\mu}_i^A - \tilde{\mu}_i^B$, yielding

$$d\tilde{s}_i = \frac{1}{\tilde{\theta}_i} du_i - \frac{\bar{\tilde{\mu}}_i}{\tilde{\theta}_i} dm_i^A \tag{9}$$

It is important to realize that these intensive variables are *estimators* of the ensemble temperature and chemical potential, due to the fact that their equilibrium average yields [12],

$$\left\langle \frac{1}{\tilde{\theta}_i} \right\rangle_T = \frac{1}{T} \tag{10}$$

$$\left\langle \frac{\tilde{\bar{\mu}}_i}{\tilde{\theta}_i} \right\rangle_T = \frac{\bar{\mu}}{T} \tag{11}$$

where the macroscopic exchange chemical potential is defined as $\bar{\mu} \equiv \mu^A - \mu^B$, by analogy with the mesoscopic counterpart.

According to Refs. [11], [12], Eq. (9) cannot be trivially inverted to express u_i as a function of $\tilde{s}_i$ and m_i^A, due to the fact that the traditional macroscopic thermodynamic relations transform as distributions when formulated at the mesoscale. Effectively, by demanding that the physical equilibrium distribution is invariant under a change of independent variables, $P(\tilde{\Gamma})d\tilde{\Gamma} = P(\Gamma)d\Gamma$, we can introduce the *dressed* variables $\Gamma \equiv \left(\{s_i\}, \{m_i^A\} \right)$ from the relation,

$$P_{\text{eq}}(\Gamma) = P_{\text{eq}}\left(\{s_i\}, \{m_i^A\} \right) \propto e^{-\sum\limits_{i=1}^{N} \left[u_i\left(s_i, m_i^A\right) - Ts_i \right] / (k_B T)} \tag{12}$$

where we have introduced s_i as the so-called *dressed* particle entropy, related to the bare particle entropy by

$$s_i = \tilde{s}_i - k_B \ln J \tag{13}$$

with the Jacobian,

$$J\left(u_i, m_i^A\right) = \left. \frac{\partial s_i}{\partial u_i} \right|_{m_i^A} \tag{14}$$

From Eq. (13), the relationship between the bare and dressed temperatures follows (see Eq. (17) of Ref. [12]),

$$\frac{1}{\tilde{\theta}_i} = \frac{1}{\theta_i} + k_B \left. \frac{\partial}{\partial u_i} \ln J \right|_{m_i^A} \tag{15}$$

Therefore, the thermodynamic relationship in Eq. (9) transforms into

$$du_i = \theta_i ds_i + \bar{\mu}_i dm_i^A \tag{16}$$

where $\bar{\mu}_i$ is the dressed exchange chemical potential,

$$\frac{\tilde{\bar{\mu}}_i}{\tilde{\theta}_i} = \frac{\bar{\mu}_i}{\theta_i} - k_B \left. \frac{\partial}{\partial m_i^A} \ln J \right|_{u_i} \tag{17}$$

The dressed variables are different estimators of the ensemble properties, i.e.,

$$\langle \theta_i \rangle_T = T \tag{18}$$

$$\langle \bar{\mu}_i \rangle_T = \bar{\mu} \tag{19}$$

Notice that the difference between dressed and bare variables is of the order of magnitude of the fluctuations, which should vanish with the size of the mesoparticles as $k_B/C_V \to 0$, with C_V being the mesoparticle heat capacity. In what follows, we require both the dressed and bare representations of the variables.

2.2 Heat and diffusive fluxes

From the exponent on the right-hand side of Eq. (3), we identify the free energy functional of the system, namely

$$\tilde{\mathcal{F}} = \sum_{i=1}^{N} \left[u_i - T\tilde{s}_i\left(u_i, m_i^A\right) \right] \tag{20}$$

Notice that this functional corresponds to the canonical ensemble and contains information about reservoir properties, i.e., the temperature T, which differs from the fluctuating particle temperature θ. In this form, we have arbitrarily chosen u_i and m_i^A as the independent variables, so that $\tilde{s}_i$ is automatically the bare entropy. As in Refs. [24], [25], we demand that the dissipative processes for the energy and material exchange between mesoparticles, in the absence of fluctuations, drive $\tilde{\mathcal{F}}$ to a minimum, for the Second Law of Thermodynamics to be satisfied at the mesoscopic level also, i.e.,

$$\dot{\tilde{\mathcal{F}}} < 0 \tag{21}$$

where the dot represents time-differentiation. Thus,

$$\sum_{i=1}^{N} \left[\dot{u}_i - T\dot{\tilde{s}}_i \right] < 0 \tag{22}$$

The equivalence of such statement and the traditional positiveness of the entropy production has been shown in Ref. [12]. Here, we will proceed straightforwardly from Eq. (22). As the independent variables are u_i and m_i, from Eq. (9), we can write

$$\dot{\tilde{s}}_i = \frac{1}{\bar{\theta}_i} \dot{u}_i - \frac{\bar{\bar{\mu}}_i}{\bar{\theta}_i} \dot{m}_i^A \tag{23}$$

Thus,

$$\sum_{i=1}^{N} \left[\dot{u}_i - T \left(\frac{1}{\bar{\theta}_i} \dot{u}_i - \frac{\bar{\bar{\mu}}_i}{\bar{\theta}_i} \dot{m}_i^A \right) \right] < 0 \tag{24}$$

The conserved quantities u_i and m_i follow some dynamic equations, which we aim at deriving eventually. On the one hand, the First Law of Thermodynamics also holds at the mesoscopic level,

$$\mathrm{d}u_i = \mathrm{d}q_i + \mathrm{d}W_i \tag{25}$$

where q_i and W_i are, respectively, the total heat transferred by mesoparticle i and the work done on mesoparticle i by the mechanical forces. Hence,

$$\dot{u}_i = \dot{q}_i + \dot{W}_i \tag{26}$$

Since the mesoparticles are static, no mechanical work is exerted and, as a consequence, $\dot{W}_i = 0$. Furthermore, separating the heat flux $\dot{q}_i$ into pairwise contributions, we arrive at

$$\dot{u}_i = \sum_{j \neq i} \dot{q}_{ij} \tag{27}$$

namely, the irreversible energy exchange produced between particles is due to the exchange of mesoscopic heat. On the other hand, we can similarly assume that the irreversible material exchanges between particles are due to pairwise diffusive fluxes, i.e.,

$$\dot{m}_i^A = \sum_{j \neq i} J_{ij}^A \tag{28}$$

The interparticle fluxes satisfy $\dot{q}_{ij} = -\dot{q}_{ji}$ and $J_{ij}^A = -J_{ji}^A$, due to property conservation. Then, from Eq. (24), and using Eqs. (27) and (28), we can write,

$$\sum_{i=1}^{N} \left[\sum_{j \neq i} \dot{q}_{ij} - T \left(\frac{1}{\bar{\theta}_i} \sum_{j \neq i} \dot{q}_{ij} - \frac{\bar{\bar{\mu}}_i}{\bar{\theta}_i} \sum_{j \neq i} J_{ij}^A \right) \right] < 0 \tag{29}$$

To develop this equation further, we can first separate the summation over $j \neq i$ into two contributions, namely, $j < i$ and $j > i$. Second, focusing on the second contribution, we can change the order of summation in such a way that $\sum_{i,j>i} \ldots = \sum_{j,i<j} \ldots$. Third, we can re-label the dummy indices $i \leftrightarrow j$ and use the change of sign of $\dot{q}_{ij}$ and J_{ij}^A under this permutation, to arrive at,

$$\sum_{i=1}^{N} \sum_{j<i} \left[T\left(\frac{1}{\bar{\theta}_j} - \frac{1}{\bar{\theta}_i} \right) \dot{q}_{ij} + T\left(\frac{\bar{\bar{\mu}}_i}{\bar{\theta}_i} - \frac{\bar{\bar{\mu}}_j}{\bar{\theta}_j} \right) J_{ij}^{\mathrm{A}} \right] < 0 \tag{30}$$

As the inequality must be satisfied irrespective of the number of pairs, we arrive to a more restrictive condition for every pair, i.e.,

$$\left[T\left(\frac{1}{\bar{\theta}_j} - \frac{1}{\bar{\theta}_i} \right) \dot{q}_{ij} + T\left(\frac{\bar{\bar{\mu}}_i}{\bar{\theta}_i} - \frac{\bar{\bar{\mu}}_j}{\bar{\theta}_j} \right) J_{ij}^{\mathrm{A}} \right] < 0 \tag{31}$$

From Eq. (31), we can identify the thermodynamic forces as

$$Y_{ij}^u = -\left(\frac{1}{\bar{\theta}_j} - \frac{1}{\bar{\theta}_i} \right) \tag{32}$$

$$Y_{ij}^m = -\left(\frac{\bar{\bar{\mu}}_i}{\bar{\theta}_i} - \frac{\bar{\bar{\mu}}_j}{\bar{\theta}_j} \right) \tag{33}$$

Notice that the thermodynamic forces are defined in terms of the bare intensive variables. Furthermore, from Eqs. (10) and (11) we can see that their equilibrium average exactly vanishes.

According to Onsager's linear non-equilibrium thermodynamics [26], the heat and diffusive fluxes are defined as linear combinations of the thermodynamic forces sharing the same tensorial nature (Curie's principle), which turns Eq. (31) into a quadratic expression in terms of the Y_{ij}'s. The implications of the inequality in Eq. (31) will be the subject of a later analysis. For our example, we thus write,

$$\dot{q}_{ij} = L_{ij}^{uu} Y_{ij}^u + L_{ij}^{um} Y_{ij}^m \tag{34}$$

$$J_{ij}^{\mathrm{A}} = L_{ij}^{mu} Y_{ij}^u + L_{ij}^{mm} Y_{ij}^m \tag{35}$$

where $L_{ij}^{uu}, L_{ij}^{um}, L_{ij}^{mu}$, and L_{ij}^{mm} are coefficients representing the mesoscopic equivalent of Onsager's phenomenological coefficients. Notice that Eqs. (34) and (35) allow for a dynamic coupling between energy and material exchange. The inequality in Eq. (31) restricts the range of allowed values for these Onsager's phenomenological coefficients. Notice that, we discussed the simplified dynamics in Ref. [24], in which $L_{ij}^{um} = L_{ij}^{mu} = 0$, corresponding to dynamically decoupled fluxes between interacting mesoscopic particles.

As a concluding remark, we comment on the usual distinction between the *heat flux* and *measurable heat flux* in the literature (see, e.g., [26], [30]). Theoretically, this distinction is related to what one would measure in a temperature gradient subject to the condition $\nabla \mu_T^\alpha = 0$. Thermodynamically, $\nabla \mu_T^\alpha$ is an object defined from the relation [26],

$$T \mathrm{d}\left(\frac{\mu^\alpha}{T} \right) \equiv \mathrm{d}\mu_T^\alpha - \frac{h^\alpha}{T} \mathrm{d}T \tag{36}$$

where h^α is the enthalpy per unit of mass of species α. Then, in classical non-equilibrium thermodynamics, from the entropy production equation it follows that the *measurable heat flux* can be defined as,

$$\dot{q}' = \dot{q} - \sum_\alpha h^\alpha J^\alpha \tag{37}$$

However, Eqs. (36) and (37) are only valid at the macroscopic level, i.e., with regards to the overall behavior of the ensemble of mesoparticles, independently of the form of Eqs. (34) and (35). For their validity, it is required that the spatial differences in the thermodynamic intensive variables are sufficiently small so that only the linear terms need to be retained, in view of Eq. (36). In Appendix A we show that the distinction between heat flux and a measurable counterpart at the level of the mesoparticles cannot be made. Only, if additional conditions on the size of the differences between particle temperatures apply, one can define a $\dot{q}'_{ij}$ analogue to the macroscopic measurable heat flux, in Eq. (37). In conclusion, as the dynamics of the fluxes is well defined by Eqs. (34) and (35)

and there is no conceptual gain in introducing an interparticle measurable heat flux at the mesoscopic level, where the measure does not occur, we will not proceed further with this analogy.

2.3 Dynamics of energy and mass exchange of static mesoparticles

To the form given in Eqs. (34) and (35) for the systematic component of the dynamics, following the general GenDPDE-M scheme of Refs. [24], [25], we now add the effect of the thermal agitation through random fluxes, in the spirit of the so-called *fluctuating hydrodynamics* of Landau and Lifshitz [3]. We thus propose the complete EoM for static mesoparticles in a discrete form,

$$u'_i = u_i + \sum_{j \neq i} \dot{q}_{ij} \delta t + \sum_{j \neq i} \delta u^R_{ij} \tag{38}$$

$$m^{A'}_i = m^A_i + \sum_{j \neq i} J^A_{ij} \delta t + \sum_{j \neq i} \delta m^R_{ij} \tag{39}$$

In Eqs. (38) and (39), prime and non-prime variables refer to the time $t + \delta t$ and t, respectively; δt is the timestep, and δu^R_{ij} and δm^R_{ij} are random contributions to the internal energy and mass of the embedded physical species A, respectively. Due to conservation, $\delta u^R_{ij} = -\delta u^R_{ji}$ and $\delta m^R_{ij} = -\delta m^R_{ji}$ are also satisfied. In the same spirit as with the linear relations of Eqs. (34) and (35), the random terms are also given by a linear combination of the form,

$$\delta u^R_{ij} = \left(\sigma^{uu}_{ij} \Omega^u_{ij} + \sigma^{um}_{ij} \Omega^m_{ij} \right) \delta t^{1/2} \tag{40}$$

$$\delta m^R_{ij} = \left(\sigma^{mu}_{ij} \Omega^u_{ij} + \sigma^{mm}_{ij} \Omega^m_{ij} \right) \delta t^{1/2} \tag{41}$$

where Ω^u_{ij} and Ω^m_{ij} are normalised Gaussian numbers for each pair of particles with the properties

$$\langle \Omega^{u,m}_{ij} \rangle = 0 \tag{42}$$

$$\langle \Omega^u_{ij}(t) \Omega^u_{kl}(t') \rangle = \langle \Omega^m_{ij}(t) \Omega^m_{kl}(t') \rangle = \left(\delta_{ik} \delta_{jl} - \delta_{il} \delta_{jk} \right) \delta_{tt'} \tag{43}$$

with

$$\langle \Omega^u_{ij}(t) \Omega^m_{kl}(t') \rangle = 0 \tag{44}$$

The coefficients σ^{uu}_{ij}, σ^{um}_{ij}, σ^{mu}_{ij}, and σ^{mm}_{ij} are the amplitudes of the thermal fluctuations, which will be set by the corresponding FD theorem. Equations (38) and (39) are complemented by the mass constraint in Eq. (1), i.e.,

$$m^{B'}_i = m_i - m^{A'}_i > 0 \tag{45}$$

as m_i is kept constant in GenDPDE-M. The EoM in Eqs. (38) and (39) can be written in a more compact form using matrix notation, i.e.,

$$\mathbf{x}_i' = \mathbf{x}_i + \sum_{j \neq i} \mathbf{L}_{ij} \cdot \mathbf{Y}_{ij} \delta t + \sum_{j \neq i} \boldsymbol{\sigma}_{ij} \cdot \boldsymbol{\Omega}_{ij} \delta t^{1/2} \tag{46}$$

where we have defined the vectors for the mesoscopic state, $\mathbf{x}_i$, thermodynamic forces, $\mathbf{Y}_{ij}$, and random contributions, $\boldsymbol{\Omega}_{ij}$, as

$$\mathbf{x}_i = \begin{pmatrix} u_i \\ m^A_i \end{pmatrix} \quad \mathbf{Y}_{ij} = \begin{pmatrix} Y^u_{ij} \\ Y^m_{ij} \end{pmatrix} \quad \boldsymbol{\Omega}_{ij} = \begin{pmatrix} \Omega^u_{ij} \\ \Omega^m_{ij} \end{pmatrix} \tag{47}$$

together with the matrices of Onsager's phenomenological coefficients, $\mathbf{L}_{ij}$, and the amplitudes of the random contributions, $\boldsymbol{\sigma}_{ij}$, according to

$$\mathbf{L}_{ij} = \begin{pmatrix} L^{uu}_{ij} & L^{um}_{ij} \\ L^{mu}_{ij} & L^{mm}_{ij} \end{pmatrix} \quad \boldsymbol{\sigma} = \begin{pmatrix} \sigma^{uu}_{ij} & \sigma^{um}_{ij} \\ \sigma^{mu}_{ij} & \sigma^{mm}_{ij} \end{pmatrix} \tag{48}$$

The mesoscopic transport coefficients in $\mathbf{L}_{ij}$ and the amplitudes of the random terms in $\boldsymbol{\sigma}_{ij}$ are linked together by the general FD theorem,

$$\boldsymbol{\sigma}_{ij} \cdot \boldsymbol{\sigma}_{ij}^T = k_B \left(\mathbf{L}_{ij} + \mathbf{L}_{ij}^T \right) \tag{49}$$

which is derived in Appendix B. In Eq. (49), the superscript ^{T} represents the *transposed* matrix. Moreover, in Appendix C we demonstrate that the ORR are also a consequence of DB, which implies that

$$\mathbf{L}_{ij}^T = \mathbf{L}_{ij} \tag{50}$$

For a binary mixture, this simply reduces to

$$L_{ij}^{um} = L_{ij}^{mu} \tag{51}$$

Due to this symmetry, Eq. (49) implies that

$$\left(\sigma_{ij}^{uu} \right)^2 + \left(\sigma_{ij}^{um} \right)^2 = 2k_B \kappa_{ij}$$

$$\left(\sigma_{ij}^{mu} \right)^2 + \left(\sigma_{ij}^{mm} \right)^2 = 2k_B Ð_{ij} \tag{52}$$

$$\sigma_{ij}^{uu} \sigma_{ij}^{mu} + \sigma_{ij}^{um} \sigma_{ij}^{mm} = 2k_B L_{ij}^{um}$$

where we introduced more natural notation for the coefficients, namely,

$$L_{ij}^{uu} \equiv \kappa_{ij} \tag{53}$$

$$L_{ij}^{mm} \equiv Ð_{ij} \tag{54}$$

Here, κ_{ij} can be regarded as the mesoscopic thermal conductivity coefficient, while $Ð_{ij}$ would be the mesoscopic Maxwell–Stefan diffusion coefficient [27]. Next, for convenience, we introduce the positive-definite coupling constants k_u and k_m from the relations,

$$\left(\sigma_{ij}^{uu} \right)^2 \equiv k_u \kappa_{ij} \tag{55}$$

$$\left(\sigma_{ij}^{mm} \right)^2 \equiv k_m Ð_{ij} \tag{56}$$

Equation (52) thus become

$$k_u \kappa_{ij} + \left(\sigma_{ij}^{um} \right)^2 = 2k_B \kappa_{ij}$$

$$k_m Ð_{ij} + \left(\sigma_{ij}^{mu} \right)^2 = 2k_B Ð_{ij} \tag{57}$$

$$\sqrt{k_u \kappa_{ij}} \; \sigma_{ij}^{mu} + \sqrt{k_m Ð_{ij}} \; \sigma_{ij}^{um} = 2k_B L_{ij}^{um}$$

These equations then can be solved to find the parameters involved in the coupling dynamics, i.e., L_{ij}^{um}, σ_{ij}^{um}, and σ_{ij}^{mu}, as functions of κ_{ij}, $Ð_{ij}$, k_u, and k_m. We obtain for the noise amplitudes,

$$\sigma_{ij}^{um} = \sqrt{(2k_B - k_u) \kappa_{ij}} \tag{58}$$

$$\sigma_{ij}^{mu} = -\sqrt{(2k_B - k_m) Ð_{ij}} \tag{59}$$

Moreover, the cross-coefficient takes the form,

$$L_{ij}^{um} = \sqrt{\kappa_{ij} Ð_{ij}} \left(-\sqrt{\frac{k_u}{2k_B} - \frac{k_u k_m}{4k_B^2}} + \sqrt{\frac{k_m}{2k_B} - \frac{k_u k_m}{4k_B^2}} \right) \tag{60}$$

It is important to note that the amplitudes of the random terms are not unequivocally determined by simply fixing κ_{ij}, $Đ_{ij}$ and L_{ij}^{um}. Effectively, σ_{ij}^{uu}, σ_{ij}^{mm}, σ_{ij}^{um}, and σ_{ij}^{mu} additionally depend upon the two coupling constants k_u and k_m in such a way that there exists a multiplicity of values of these that are compatible with the same dissipative processes described by the coefficients κ_{ij}, $Đ_{ij}$ and L_{ij}^{um}. This fact indicates that, at the current level of description of Langevin-like equations, one still has an additional degree of freedom in the choice of the relative amplitude of the random currents, keeping κ_{ij}, $Đ_{ij}$, and L_{ij}^{um} fixed nevertheless, without violating DB. At this point, if there is no additional physical information that could allow us to elucidate the values of k_u and k_m, we are forced to make an educated choice, as the overall macroscopic processes are not affected. Moreover, notice that we have chosen $\sigma_{ij}^{um}\sigma_{ij}^{mu} < 0$ as it is the only physically meaningful solution of Eq. (49) for the dynamic coupling of the mass and energy fluxes.

Next, in view of Eq. (31), Onsager's coefficients must satisfy the following sign conditions,

$$L_{ij}^{uu} > 0 \tag{61}$$

$$L_{ij}^{mm} > 0 \tag{62}$$

$$L_{ij}^{uu}L_{ij}^{mm} - \left(L_{ij}^{um}\right)^2 > 0 \tag{63}$$

which imply that $\kappa_{ij} > 0$ and $Đ_{ij} > 0$. In addition, from Eqs. (55) and (56) it also follows that $k_u > 0$ and $k_m > 0$. Moreover, from Eq. (63) we also find that the coupling constants are subject to the following inequality,

$$\frac{k_u + k_m}{2k_B} - \frac{k_u k_m}{2k_B^2} - \sqrt{\frac{k_u k_m}{k_B^2}\left(1 - \frac{k_u + k_m}{2k_B} + \frac{k_u k_m}{4k_B^2}\right)} < 1 \tag{64}$$

Combining Eq. (64) with the definitions of the amplitudes of the random terms, Eqs. (55), (56), (58), and (59), we arrive at the identification of the physically acceptable bounds for the coupling constants, namely,

$$k_u \in \left[0, 2k_B\right] \tag{65}$$

$$k_m \in \left[0, 2k_B\right] \tag{66}$$

The choice $k_u = k_m$ implies that $L_{ij}^{um} = 0$, and no coupling between the energy and mass transport occurs. However, notice that under this choice σ_{ij}^{um} and σ_{ij}^{mu} may still be different from zero. As we mentioned, this situation has no effect on the overall dynamics of the system. Only in the case where $k_u = k_m = 2k_B$, do all coefficients in Eqs. (58)–(60) identically vanish. This latter situation exactly corresponds to the decoupled GenDPDE-M method presented in our prior publications [24], [25].

2.4 The equations of motion

The dynamics of heat and mass transport, Eq. (46), with the corresponding FD relations, expressed in Eqs. (55), (56), (58) and (59), can be easily incorporated into the mechanical motion of a system of moving mesoparticles with an embedded binary mixture, because of our choice of constant mass (*cf*. Eq. (1)). The equilibrium distribution for the complete set of variables is the extension of Eq. (3) with the energy due to the mechanical degrees of freedom, i.e.,

$$P_{eq}(\tilde{\Gamma}) = P_{eq}\left(\{\mathbf{p}_i\}, \{\mathbf{r}_i\}, \{u_i\}, \{m_i^A\}\right) \propto e^{-\sum_{i=1}^{N}\left[\frac{\mathbf{p}_i^2}{2m_i} + \tilde{\mathcal{F}}(u_i, n_i, m_i^A)\right]/(k_B T)} \tag{67}$$

where the functional form of $\tilde{\mathcal{F}}$ is defined in Eq. (20). In Eq. (67), the local particle density $n_i(\{\mathbf{r}_j\})$ is defined from the particle positions, according to the expression,

$$n_i = \sum_{j \neq i} w_{ij} \tag{68}$$

where $w_{ij} \equiv w(r_{ij})$ is a smooth, monotonically decreasing ($\mathrm{d}w_{ij}/\mathrm{d}r_{ij} < 0$), non-negative, spherically symmetric weighting function. It vanishes for an interparticle distance, $r_{ij} \equiv |\mathbf{r}_i - \mathbf{r}_j|$, such that $r_{ij} \geq R_{\mathrm{cut}}$, where R_{cut} is the cut-off range. Unlike the other weighting functions defined in this work, w_{ij} is normalized so that $4\pi \int_0^{R_{\mathrm{cut}}} w(r)r^2 \mathrm{d}r = 1$, for convenience. Notice that n_i is in fact a measure of the particle volume $v_i \equiv 1/n_i$, which is directly connected to the compression-expansion work implicit of the local thermodynamic description.

Due to the spatial motion of the particles, here we have to explicitly take into account that the dissipative parameters are space-dependent, i.e.,

$$\kappa_{ij} = \kappa \, \omega^u(r_{ij}) \tag{69}$$

$$\mathcal{D}_{ij} = \mathcal{D} \, \omega^m(r_{ij}) \tag{70}$$

where $\omega^u(r_{ij})$ and $\omega^m(r_{ij})$ are smooth, monotonically decreasing, non-negative, and spherically symmetric weighting functions. They vanish for $r_{ij} \geq R_{\mathrm{cut}}^u$ and $r_{ij} \geq R_{\mathrm{cut}}^m$, with R_{cut}^u and R_{cut}^m being the cutoff distances for $\omega^u(r_{ij})$ and $\omega^m(r_{ij})$, respectively. The energy and mass weighting functions are defined independently of the density weighting function defined in Eq. (68). From Eqs. (69) and (70), using Eq. (60), we can furthermore highlight the spatial dependence of the cross-coefficient L_{ij}^{um}, i.e.,

$$L_{ij}^{um} = L^{um} \sqrt{\omega^u(r_{ij})\omega^m(r_{ij})} \tag{71}$$

where

$$L^{um} = \sqrt{\kappa \, \mathcal{D}} \left(-\sqrt{\frac{k_u}{2k_B} - \frac{k_u k_m}{4k_B^2}} + \sqrt{\frac{k_m}{2k_B} - \frac{k_u k_m}{4k_B^2}} \right) \tag{72}$$

As the positions are slow variables compared to u_i, m_i^{A} and the particle velocities $\mathbf{v}_i = \mathbf{p}_i/m_i$, we can safely substitute the expressions in Eqs. (69) and (70) into the FD relations Eqs. (55), (56), (58), and (59), without further change.

The EoM for N mesoparticles in the coupled GenDPDE-M method are identical to those of Ref. [24], i.e.,

$$\mathbf{r}_i' = \mathbf{r}_i + \frac{\mathbf{p}_i}{m_i}\delta t \tag{73}$$

$$\mathbf{p}_i' = \mathbf{p}_i + \sum_{j\neq i} \mathbf{f}_{ij}^C \delta t + \sum_{j\neq i} \mathbf{f}_{ij}^D \delta t + \sum_{j\neq i} \delta \mathbf{p}_{ij}^R \tag{74}$$

$$u_i' = u_i - \frac{1}{2}\sum_{j\neq i}\left(\frac{\mathbf{p}_i}{m_i} - \frac{\mathbf{p}_j}{m_j}\right) \cdot \mathbf{f}_{ij}^C \delta t \tag{75}$$

$$-\frac{1}{2}\sum_{j\neq i}\left(\frac{\mathbf{p}_i}{m_i} - \frac{\mathbf{p}_j}{m_j}\right) \cdot \mathbf{f}_{ij}^D \delta t$$

$$-\frac{1}{2}\sum_{j\neq i}\left(\frac{\mathbf{p}_i}{m_i} - \frac{\mathbf{p}_j}{m_j}\right) \cdot \delta \mathbf{p}_{ij}^R$$

$$-\frac{1}{2m_i}\sum_{j\neq i}\sum_{l\neq i}\delta \mathbf{p}_{ij}^R \cdot \delta \mathbf{p}_{il}^R \tag{76}$$

$$+\sum_{j\neq i}\dot{q}_{ij}\delta t + \sum_{j\neq i}\delta u_{ij}^R$$

$$m_i^{\mathrm{A}'} = m_i^{\mathrm{A}} + \sum_{j\neq i}J_{ij}^{\mathrm{A}}\delta t + \sum_{j\neq i}\delta m_{ij}^R$$

$$m_i^{\mathrm{B}'} = m_i - m_i^{\mathrm{A}'} \tag{77}$$

The dynamic coupling between mass and energy transport is taken into account through the form of the heat and mass fluxes, given by Eqs. (34) and (35), together with the random fluxes, Eqs. (40) and (41). For completeness, in Eqs. (74) and (75),

$$\mathbf{f}_{ij}^{C} = -\left(\frac{\pi_i}{n_i^2} + \frac{\pi_j}{n_j^2} \right) \frac{\mathrm{d}w_{ij}}{\mathrm{d}r_{ij}} \mathbf{e}_{ij} \tag{78}$$

is the conservative force between a pair of mesoparticles i and j, where π_i the particle pressure that follows from the free energy of the EoS for the mesoparticle. Note that the particle pressure will contribute to the overall system pressure as an *excess* pressure, as there is always an ideal contribution due to the thermal agitation of the mesoparticles. This point is important when defining the particle EoS targeting a given specific *macroscopic* thermodynamic behavior. In Eq. (78), $\mathbf{e}_{ij} \equiv \mathbf{r}_{ij}/r_{ij}$. Further, the friction force takes the usual DPD form (see, e.g., [12]),

$$\mathbf{f}_{ij}^{D} = -\gamma_{ij} \left(\frac{\mathbf{p}_i}{m_i} - \frac{\mathbf{p}_j}{m_j} \right) \cdot \mathbf{e}_{ij} \mathbf{e}_{ij} \tag{79}$$

for a pair of mesoparticles i and j. Here, $\gamma_{ij} = \gamma \, \omega^p(r_{ij})$, γ being the mesoscopic friction coefficient, and $\omega^p(r_{ij})$ being a weighting function with the same properties as the other functions in Eqs. (69) and (70), vanishing for $r_{ij} \geq R_{\mathrm{cut}}^{p}$, where R_{cut}^{p} is the cut-off range for this property. Finally, according to Ref. [24],

$$\delta\mathbf{p}_{ij}^{R} = \sqrt{k_B(\theta_i + \theta_j)\gamma_{ij}} \; \Omega_{ij}^{p} \mathbf{e}_{ij}\delta t^{1/2} \tag{80}$$

is the random contribution to the particle momentum, and Ω_{ij}^{p} is a normalised Gaussian number with analogous properties to those defined in Eqs. (42) and (43). It is very important to realize that, according to Refs. [12], [24], Eq. (80) explicitly depends upon the dressed temperature. The latter can be written in terms of the bare temperature, using Eq. (15).

2.5 Particle thermodynamic model

As a representative example, we aim at describing a *macroscopic* system whose thermodynamics is given by the vdW mixture model, based on the vdW EoS [31], and the one-fluid (1f) conformational solution theory [32], which treats a mixture as a pseudo-fluid with composition-dependent parameters.

Specifically, the vdW EoS a_i and b_i parameters of the mesoparticle i are given by the combining rules [32], [33]

$$a_i = \sum_\alpha \sum_\beta x_i^\alpha x_i^\beta \sqrt{a_\alpha a_\beta} \tag{81}$$

$$b_i = \sum_\alpha x_i^\alpha b_\alpha \tag{82}$$

where a_α and b_α are the vdW EoS parameters of the embedded physical species α, and $x_i^\alpha = \mathcal{N}_i^\alpha / \mathcal{N}_i$ is its molar fraction.

Then, for the particle pressure needed for evaluation of the conservative force, Eq. (78), we propose a corrected vdW EoS by the subtraction of the ideal gas contribution due to the mesoparticle agitation, namely,

$$\begin{aligned} \pi_i &= \frac{\mathcal{N}_i n_i k_B \theta_i}{1 - \bar{b}_i n_i} - \bar{a}_i n_i^2 - k_B \theta_i n_i \\ &\equiv \pi_i^{\mathrm{EoS}} - k_B \theta_i n_i \end{aligned} \tag{83}$$

where [25],

$$\bar{a}_i \equiv \mathcal{N}_i^2 a_i \tag{84}$$

$$\bar{b}_i \equiv \mathcal{N}_i b_i \tag{85}$$

We have chosen to express the mesoparticle thermodynamics in terms of dressed variables, although the physically relevant properties of the model can equally be expressed in terms of bare variables. Effectively, if

Eq. (15) is taken into account, together with the fact that the bare pressure is related to the dressed one through the relation,

$$\frac{\tilde{\pi}_i}{\tilde{\theta}_i} = \frac{\pi_i}{\theta_i} + k_B \frac{\partial}{\partial n_i} \ln J \Big|_{u_i, m_i^A} \tag{86}$$

then the equilibrium probability distributions remain invariant.

Equation (83) can be derived from the appropriate particle Helmholtz free-energy f, as found in Appendix A of Ref. [25]. The expression reads

$$f_i = k_B \theta_i \sum_\alpha \mathcal{N}_i^\alpha \ln\left(\frac{\mathcal{N}_i^\alpha n_i}{(1 - \bar{b}_i n_i) n_0}\right) - \bar{a}_i n_i + C_{V,i} \theta_i - C_{V,i} \theta_i \ln\left(1 + \frac{\theta_i}{\theta_0}\right) - k_B \theta_i \ln\left(\frac{n_i}{n_0}\right) \tag{87}$$

where $C_{V,i} = \sum_\alpha \mathcal{N}_i^\alpha C_{V,i}^\alpha$ is the composition-dependent heat capacity of the mesoparticle, with $C_{V,i}^\alpha$ the constant-volume heat capacity per molecule belonging to the embedded physical species α, and $\bar{a}_i$ together with $\bar{b}_i$ are given in Eqs. (84) and (85), respectively. Notice that, we have not subtracted in Eq. (87) the contribution due to the mesoparticle agitation, as we did in the right-hand side of Eq. (A3) of Ref. [25]. The parameters n_0 and θ_0 are included for dimensional consistency, and will be considered as constants.

Therefore, to obtain the expression of the internal energy u_i, from which the temperature θ_i can be calculated, we have to first derive the particle entropy, from the usual relation $s_i = -\partial f_i / \partial \theta_i |_{n_i, \{m_i^\alpha\}}$, i.e.,

$$s_i = -k_B \sum_\alpha \mathcal{N}_i^\alpha \ln\left(\frac{\mathcal{N}_i^\alpha n_i}{(1 - \bar{b}_i n_i) n_0}\right) - C_{V,i} + C_{V,i} \ln\left(1 + \frac{\theta_i}{\theta_0}\right) + C_{V,i} \frac{\theta_i/\theta_0}{1 + \theta_i/\theta_0} + k_B \ln\left(\frac{n_i}{n_0}\right) \tag{88}$$

Equation (A4) in Ref. [25] corresponds to the high-temperature limit $\theta_i/\theta_0 \gg 1$ of this expression. We will also take such limit in this work, to make our expressions in more accordance with real gases. However, before we simplify our expressions, we can calculate the form of the internal energy u_i from Eq. (87) using $u_i = f_i + \theta_i s_i$, which reads,

$$u_i = C_{V,i} \theta_i \frac{\theta_i/\theta_0}{1 + \theta_i/\theta_0} - \bar{a}_i n_i \tag{89}$$

Finally, the chemical potential of species α is obtained from Eq. (87) through differentiation with respect to m_i^α, where one obtains,

$$\mu_i^\alpha = \frac{1}{\bar{m}_\alpha} \left\{ k_B \theta_i \left[\ln\left(\frac{\mathcal{N}_i^\alpha n_i}{(1 - \bar{b}_i n_i) n_0}\right) + 1 + \frac{\mathcal{N}_i n_i}{1 - \bar{b}_i n_i} b_\alpha\right] - 2n_i \sum_\beta \mathcal{N}_i^\beta \sqrt{a_\alpha a_\beta} + C_{V,i}^\alpha \theta_i \left[1 - \ln\left(1 + \frac{\theta_i}{\theta_0}\right)\right] \right\} \tag{90}$$

From a practical point of view, we are using the simplified expressions for the internal energy as well as the chemical potentials in the high temperature limit $\theta_i/\theta_0 \gg 1$, thus obtaining our final expressions required for the simulations, i.e.,

$$u_i = C_{V,i} \theta_i - \bar{a}_i n_i \tag{91}$$

for the internal energy, and

$$\mu_i^\alpha = \frac{1}{\bar{m}_\alpha} \left[\left(k_B + C_{V,i}^\alpha\right) \theta_i + k_B \theta_i \ln\left(\frac{\mathcal{N}_i^\alpha n_i}{(1 - \bar{b}_i n_i) n_0}\right) + \frac{k_B \theta_i \mathcal{N}_i n_i}{1 - \bar{b}_i n_i} b_\alpha - 2n_i \sum_\beta \mathcal{N}_i^\beta \sqrt{a_\alpha a_\beta} - C_{V,i}^\alpha \theta_i \ln\left(\frac{\theta_i}{\theta_0}\right)\right] \tag{92}$$

for the chemical potential.

2.5.1 Bare variables

Since the thermodynamic forces in Eqs. (32) and (33) are expressed in terms of bare variables, the explicit expressions for the bare temperature as well as the bare chemical potentials are required. To this end, let us first consider the form of the Jacobian of the transformation, given in Eq. (14), already in the high temperature limit,

$$J = \left.\frac{\partial s_i}{\partial u_i}\right|_{n_i,\{m_i^\alpha\}} = \left.\frac{\partial s_i}{\partial \theta_i}\right|_{n_i,\{m_i^\alpha\}} \times \left.\frac{\partial \theta_i}{\partial u_i}\right|_{n_i,\{m_i^\alpha\}} = \frac{1}{\theta_i} \tag{93}$$

where use has been made of Eqs. (88) and (91) to calculate the derivatives. Therefore, from Eq. (91), using Eq. (15),

$$\frac{1}{\tilde{\theta}_i} = \frac{1}{\theta_i}\left(1 - \frac{k_B}{C_{V,i}}\right) \tag{94}$$

In the same way, from Eq. (17), using again Eq. (91), one finds,

$$\frac{\tilde{\mu}_i^\alpha}{\tilde{\theta}_i} = \frac{\mu_i^\alpha}{\theta_i} + \frac{k_B}{C_{V,i}\theta_i}\frac{1}{\bar{m}_\alpha}\left[2n_i\sum_\beta \mathcal{N}_i^\beta\sqrt{a_\alpha a_\beta} - C_{V,i}^\alpha\theta_i\right] \tag{95}$$

The vdW EoS, and in fact all properties derived from Eq. (87), is not defined for $\bar{b}_i n_i > 1$. Thus, we employed an extension to avoid numerical problems, whose details are given in Refs. [11], [25].

3 Computational details

As in the decoupled GenDPDE-M method [24], [25], the EoM in Eqs. (73)–(77) were integrated by the extended Shardlow splitting algorithm, which separately discretizes the reversible and irreversible parts of the dynamics [34], [35].

We consider an embedded binary mixture of an atomic and a diatomic fluid, taking the equimolar Ar(A)/Cl$_2$(B) binary mixture as a representative example. Values of the vdW EoS parameters were determined from the critical temperature, T_c, and critical pressure, P_c, of Ar and Cl$_2$, according to [32]

$$a_\alpha = \frac{27}{64}\frac{\left(k_B T_c^\alpha\right)^2}{P_c^\alpha}$$

$$b_\alpha = \frac{1}{8}\frac{k_B T_c^\alpha}{P_c^\alpha}$$

where $T_c^{Ar} = 150.69$ K and $P_c^{Ar} = 48.63$ bar, and $T_c^{Cl_2} = 417$ K and $P_c^{Cl_2} = 79.91$ bar. GenDPDE-M simulations for the mixture were carried out at state points such that both substances would be under supercritical conditions if pure. Thus, the simulated mixture behavior is far from ideal gas conditions.

The simulations were performed using Lennard–Jones reduced units, where $m_{ref} = \bar{m}_A$, $\varepsilon_{ref} = a_A/b_A$, $\sigma_{ref} = \sqrt[3]{b_A}$ were taken as the units of mass, energy, and length, respectively, thus fixing the time unit to $t_{ref} = \sqrt{\sigma_{ref}^2 m_{ref}/\varepsilon_{ref}}$. Hence, in reduced units, $m_i^{\alpha*} \equiv m_i^\alpha/m_{ref}$, $n_i^* \equiv n_i\sigma_{ref}^3$, $\theta_i^* \equiv k_B\theta_i/\varepsilon_{ref}$, $u_i^* \equiv u_i/\varepsilon_{ref}$, $\pi_i^* \equiv \pi_i\sigma_{ref}^3/\varepsilon_{ref}$, and $t^* = t/t_{ref}$. In the following, we will use only reduced variables and drop the $*$ where confusion cannot occur. From the molecular masses of Ar and Cl$_2$, for simplicity we further set $\bar{m}_B = 2\bar{m}_A$, $C_V^A = (3/2)k_B$, $C_V^B = (5/2)k_B$, and the level of CGing $\Phi = 10$. Hence, since we chose an initial equimolar mixture, the initial composition of mesoparticle i corresponds to $\mathcal{N}_i^A = \mathcal{N}_i^B = 5$ ($m_i^A = 5$, $m_i^B = 10$), with $m_i = 15 = $ const.

We used the Lucy weighting function [36] for $w(r)$, and the quadratic weighting function [11] for $\omega^p(r)$, $\omega^u(r)$ and $\omega^m(r)$, with cut-off distances $R_{cut} = R_{cut}^p = R_{cut}^u = R_{cut}^m$. Equilibrium simulations were performed in a cubic simulation box with periodic boundary conditions (PBC) in all three directions, and with $N = 5,000$ mesoparticles. Non-equilibrium simulations were carried out in an orthorhombic simulation box of volume $V = L_x L_y L_z$, with PBC and $L_y = L_z = L_x/3$, containing $N = 9,000$ mesoparticles. Finally, we employed $\delta t = 0.005$, and varied γ, κ, Đ, k_u, and k_m, to consider different simulation scenarios.

3.1 Simulations under temperature gradient

To simulate the dependence of the Ludwig–Soret effect (thermodiffusion) with the dynamic coupling between energy and mass within the GenDPDE-M method, we modified the reverse PeX non-equilibrium method by Müller–Plathe [37], [38], often used in molecular dynamics to generate a temperature gradient while conserving the total energy and momentum. The method sets hot (h) and cold (c) regions (slabs) at prefixed x-positions in an orthorhombic simulation box, such that they are at the same distance within the box as well as across the PBC in the x-direction. Relative to L_x, the slab thickness was set small enough to have a sufficiently long section for the temperature gradient to develop and occupy most of the box, but at the same time, sufficiently large to contain enough mesoparticles so that the estimated mean temperatures minimally fluctuate. Unlike the PeX method described in Refs. [37], [38], where fast particles in the cold slab virtually collide with slow particles in the hot slab to create a net energy flux from cold to hot, here, at a given frequency f_{exc} during the simulations, the mesoparticle with the highest particle temperature in the cold slab is selected to exchange a prescribed amount of heat, $\delta q > 0$, with the mesoparticle with the lowest temperature in the hot slab. This procedure ensures that the total momentum and energy of the system remain invariant, despite the temperature gradient that develops as a consequence of the forced heat flux across the sample, which is externally controlled by the values of δq and f_{exc}. Therefore, the internal energy of the mesoparticles involved in the exchange is updated as

$$u^h = u^h + \delta q$$
$$u^c = u^c - \delta q$$

In our simulations, the virtual heat transfer between the cold and hot slabs was performed every timestep, i.e., $f_{exc} = 1$, and the value of δq was adjusted to produce a small, linear temperature gradient profile between the hot and cold slabs. The linearity of the obtained temperature profile allows us to use linear response theory, and evaluate the macroscopic thermal conductivity together with the Soret coefficient [26].

Once the system has reached steady state, the heat-flux density is calculated as

$$J_x = \frac{Q}{A\Delta t} \tag{96}$$

where $A = L_y L_z$ is the cross-sectional area of the slab, Δt is the time between the initial measuring time t_1 and the final time t_2, during which the exchanged energy is accumulated into $Q = \sum_{t_1}^{t_2} \delta q$. Since δq is a constant, Eq. (96) becomes

$$J_x = \frac{1}{A}\frac{\delta q}{\delta t} \tag{97}$$

The macroscopic thermal conductivity λ is then defined from the relation,

$$\lambda = -\lim_{\frac{dT}{dx}\to 0}\frac{J_x}{dT/dx} \tag{98}$$

where it is assumed that the material flux is zero at steady state. Here, $T(x) = \langle\theta(x)\rangle$ and dT/dx is the average particle temperature gradient in the x-direction, taken over measures at different times while in steady state. In Eq. (98), the $dT/dx \to 0$ formally expresses the necessity of a very small gradient to achieve the linearity of the response [26]. To determine the local values of the temperature, we divided the space between the slabs into several narrow bins and evaluated the local average of the dressed temperature, $\langle\theta_i\rangle$, over the particles within each bin. Notice that we use the dressed temperature here because it is an estimator of the equilibrium temperature, in view of Eq. (18). After taking different snapshots of the temperature distribution along the sample, we averaged them and evaluated the temperature gradient from the mean profile, using a linear regression over most of the central section between the slabs. Then, the thermal conductivity λ is obtained from Eq. (98). Notice that while the heat flux is externally imposed and has no variability, the determination of the temperature gradient is affected by numerical uncertainty, which propagates to the reported value of λ.

Equation (98) follows the criterion of Refs. [30], [38] in which, in a multicomponent system, λ is defined with the material fluxes set to zero, as it agrees with a simple experimental setup. Hence, the relationship between

the heat transported and the temperature gradient follows from Fourier's law, but also includes the effects of the coupling between the energy and mass transport through the concentration gradient. Other criteria could be invoked [26], in which the thermal conductivity is defined also from Eq. (98), but under the assumption that either $\nabla \bar{\mu} = 0$ or $\nabla(\bar{\mu}/T) = 0$. Although the values for the thermal conductivity may differ, depending on the conditions chosen, the physical phenomena is invariant if the implications of these definitions are properly taken into consideration.

Finally, the Soret coefficient for embedded species B in a binary mixture is also obtained from the condition of zero material flux at steady state, and can be computed as [26]

$$s_T^B = -\frac{1}{\bar{x}^A \bar{x}^B} \frac{dx^B/dx}{dT/dx} \tag{99}$$

where $\bar{x}^A$ and $\bar{x}^B$ are the overall average molar fractions of the embedded species A and B, respectively, and dx^B/dx is the average molar fraction gradient of embedded species B in the x-direction. The Soret coefficient for embedded species A can be analogously defined. Moreover, in a binary mixture, $s_T^A = -s_T^B$. Similarly as with λ, s_T^A and s_T^B in our model are affected by the strength of the coupling between energy and mass at the mesoscale.

4 Results

In this section, we present and discuss the results of equilibrium and non-equilibrium GenDPDE-M simulations with different values for the parameters that govern the dynamic coupling between energy and mass transfer at the mesoscale. Equilibrium simulations provide numerical proof of the independence of the probability distributions from the mesoscopic transport coefficients. Non-equilibrium simulations, on the other hand, are used to explore the effects of the coupling on heat transport and thermodiffusion. Finally, the dependence of the system's properties on the level of CGing is also analyzed.
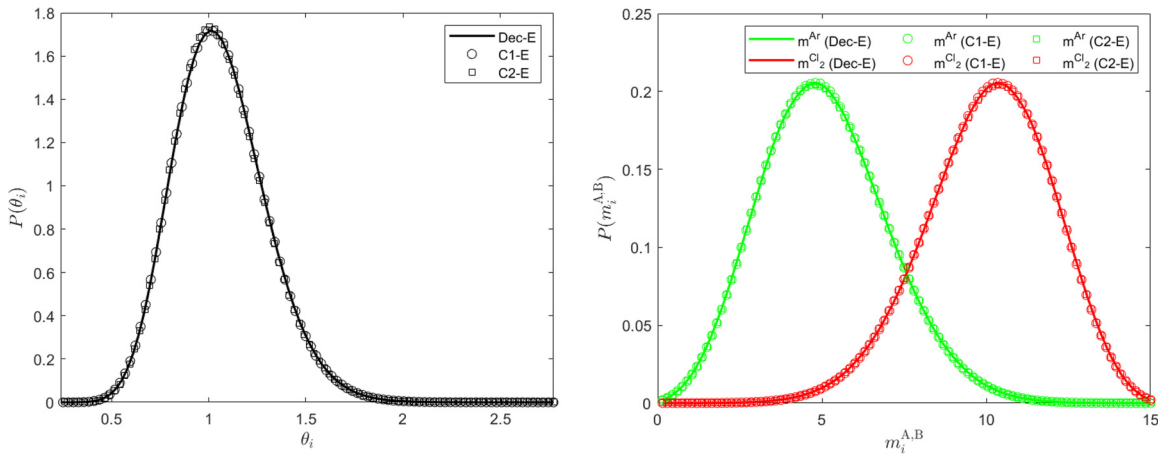
4.1 Equilibrium simulations

Three GenDPDE-M simulations of the CG equimolar Ar/Cl$_2$ binary mixture were performed for an initial temperature $T = 1.081$ and an overall system number density $c = 0.3152$, which correspond to supercritical conditions for the pure substances. In these simulations, we varied the mesoscopic dynamic coefficients γ, κ and Đ, as well as the coupling constants, k_u and k_m, as reported in Table 1. For each of these sets of parameters, we evaluated the equilibrium distributions for θ_i (dressed temperature), m_i^A and m_i^B, as shown in Figure 1. Here, test Dec-E corresponds to the decoupled case in which the values of the coupling constants were chosen to simulate the same algorithm as in Refs. [24], [25], namely, $k_u = k_m = 2k_B$, in view of Eqs. (58) and (59). Tests C1-E and C2-E, on the other hand, correspond to coupled energy-mass dynamics scenarios.

From Figure 1, we can see that $P(\theta_i)$ as well as $P(m_i^A)$ and $P(m_i^B)$ perfectly overlap for all cases, thus providing a numerical proof of consistency of the FD theorem. Effectively, since the particle thermodynamic model is the same in all tests, the system dynamics is expected to sample the same equilibrium distributions regardless of the chosen values of the mesoscopic transport coefficients and coupling constants.

Table 1: Parameters employed in equilibrium GenDPDE-M simulations. The mesoscopic transport coefficients γ, κ and Đ represent the friction, thermal conductivity and Maxwell-Stefan coefficients, respectively. The coupling constants k_u and k_m are energy and mass prefactors with the dimensions of k_B. n_{run} is the selected number of simulation timesteps.

Test	γ	κ	Đ	k_u	k_m	n_{run}
Dec-E	4.5	1.0	0.01	2.0	2.0	1×10^6
C1-E	4.5	1.0	0.01	1.0	1.5	1×10^6
C2-E	0.9	5.0	0.05	1.0	1.5	1×10^6

Figure 1: The equilibrium probability distributions of the particle temperature (top) and embedded species masses (bottom) for the CG equimolar Ar/Cl$_2$ binary mixture at an initial temperature $T = 1.081$ and system number density $c = 0.3152$, as obtained from the decoupled GenDPDE-M simulation, Dec-E, and coupled GenDPDE-M simulations C1-E and C2-E. All the distributions consistently overlap.

4.2 Non-equilibrium simulations

Non-equilibrium simulations of the CG equimolar Ar/Cl$_2$ binary mixture were carried out for an initial state $T = 0.885$ and $c = 0.5775$, corresponding again to supercritical conditions for the pure substances. Six GenDPDE-M tests were performed, in which we set $\gamma = 4.5$, $\kappa = 1$ and Đ = 5, and varied L^{um} according to the values of k_u and k_m given in Table 2. Notice that the mesoscopic Maxwell–Stefan coefficient Đ was increased with respect to the equilibrium simulations to allow the system to quickly relax to steady-state conditions, thus reducing the computational cost of the tests. A short equilibration run of $n_{equil} = 1 \times 10^5$ timesteps was performed before imposing heat transfer between the hot and cold slabs. A relaxation period of $n_{relax} = 4 \times 10^5$ timesteps was subsequently considered, after which no variation in the average temperature and concentration profiles was observed.

Similarly to the equilibrium cases, here test Dec-NE refers to a decoupled system simulating the same algorithm as in Refs. [24], [25]. As shown in Table 2, tests C1-NE, C2-NE and C3-NE consider coupled configurations with different strengths of the dynamic energy-mass coupling effect, controlled by the value of the coefficient L^{um}. Furthermore, with the aim of assessing the independence of the results from the choice of k_u and k_m provided that L^{um} is kept constant, simulations C1b-NE and C2b-NE were performed, testing identical conditions to the cases C1-NE and C2-NE, respectively, but using different values of the coupling constants.

Figure 2 shows the steady-state profiles of the local average particle dressed temperature, $T(x) = \langle \theta(x) \rangle$, which is a possible estimator of the local temperature. Notice that, if the bare temperature $\tilde{\theta}$ were used as the

Table 2: Parameters employed in non-equilibrium GenDPDE-M simulations. The coupling constants k_u and k_m are energy and mass prefactors with the dimensions of k_B. L^{um} is the mesoscopic Onsager's cross-coefficient defined in Eq. (72). n_{run} is the selected number of simulation timesteps.

Test	k_u	k_m	L^{um}	n_{run}
Dec-NE	2.0000	2.0000	0.0	1.5×10^6
C1-NE	1.5000	0.6072	−1.0	1.5×10^6
C2-NE	1.8000	0.4830	−1.5	1.5×10^6
C3-NE	0.5000	1.3929	1.0	1.5×10^6
C1b-NE	0.9000	0.1440	−1.0	1.5×10^6
C2b-NE	1.1000	0.0200	−1.5	1.5×10^6
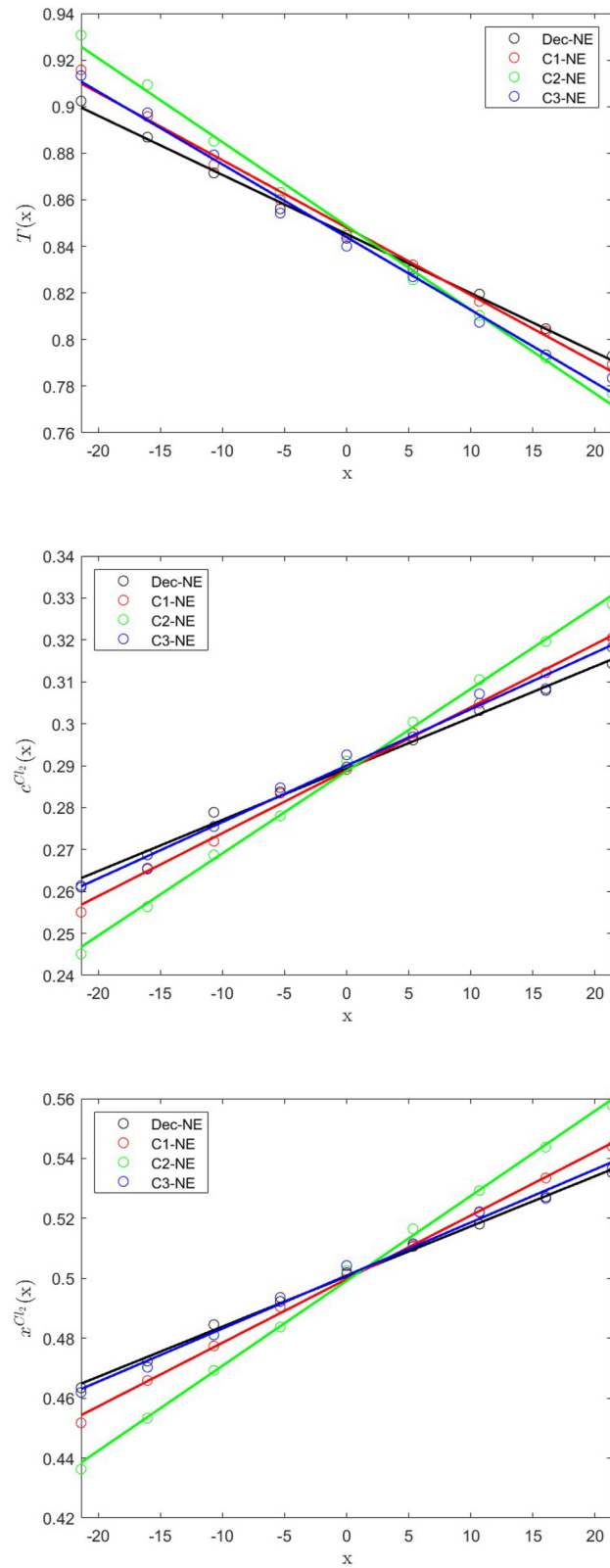
Figure 2: The x-profiles of the particle temperature (top), and the number concentration (middle) and molar fraction (bottom) of Cl_2 for the CG equimolar Ar/Cl_2 binary mixture at an initial temperature $T = 0.885$ and system number density $c = 0.5775$, as obtained from the decoupled GenDPDE-M simulation, Dec-NE, and coupled GenDPDE-M simulations C1-NE, C2-NE and C3-NE. The circles represent simulation results, while the solid lines represent linear regressions.

estimator instead, the correct temperature profile would be obtained from the relation $T(x) = \langle 1/\tilde{\theta}(x) \rangle^{-1}$. In addition, Figure 2 shows the average profiles for the number concentration, $c^B(x)$, and the molar fraction, $x^B(x)$, of Cl_2. Here, only the decoupled case Dec-NE and the coupled cases C1-NE, C2-NE and C3-NE have been considered. These profiles were obtained by dividing the x-domain between the hot and cold slabs into nine bins, and calculating averages of the quantities of interest within each bin, after reaching steady state, at a fixed frequency of $f_{samp} = 25{,}000$ timesteps, for a total of 41 snapshots. These *instantaneous profiles* were subsequently further averaged to obtain the diagrams shown in Figure 2. From this figure, we can observe that the heat flux J_x, imposed on the system via the modified PeX algorithm, not only produces a temperature gradient between the slabs, but also causes a concentration gradient to develop, in agreement with the experimental findings within the context of the Ludwig–Soret effect [26]. Furthermore, notice that the heavier species Cl_2 accumulates in the cold region of the simulation box, as expected, even for case Dec-NE. Although no dynamic coupling between mass and energy is present at the mesoscopic level, the observed material gradient for this decoupled case is due to the dependence of the particle exchange chemical potential on the space-dependent temperature, plus additional contributions due to the thermal motion of the mesoparticles. As such, the observed thermodiffusion has a purely thermodynamic origin. However, when the dynamic coupling between energy and matter is included in the model, as in cases C1-NE, C2-NE, and C3-NE, such a composition gradient is modified by the *interspecific friction* [27], gathered in the value of the cross-coefficient L^{um}.

In Figure 3 we analyze the results of the aforementioned pairs of analogous cases, namely C1-NE and C1b-NE, as well as C2-NE and C2b-NE. The temperature, concentration and molar fraction profiles observed for cases C1b-NE and C2b-NE are practically indiscernable when compared to tests C1-NE and C2-NE, respectively: this result proves that the overall macroscopic behavior of our model is indeed insensitive to the specific values of the coupling constants k_u and k_m, and depends only on the parameters κ and $Đ$ and on the coupling coefficient L^{um}.

From the profiles $T(x)$ and $x^B(x)$, we evaluated the corresponding gradients, dT/dx and dx^B/dx, using linear regressions, and computed the thermal conductivity, λ, as well as the Soret coefficient, $s_T^{Cl_2}$, as defined by Eqs. (98) and (99). The measured values of λ and $s_T^{Cl_2}$, together with the heat flux density, J_x, and the gradients dT/dx, and dx^B/dx, are provided in Table 3. We can see that the value of λ decreases with an increase in the absolute strength of the energy and mass coupling, as is to be expected, since from Eqs. (34) and (35) one could estimate that $\lambda = J_x/|\nabla T| \simeq (\kappa - (L^{um})^2/ -Đ)/T^2 +$ kinetic contributions [30]. As far as the Ludwig–Soret effect is concerned, the value of $s_T^{Cl_2}$ decreases upon increasing the mesoscopic cross-coefficient L^{um}. However, this should not be considered as a general trend, but as a result of the particular model we are considering, in which the dynamic coupling counters the thermodynamic effect caused by the temperature gradient when $L^{um} > 0$.

We observe that the measured errors in the determination of both λ and $s_T^{Cl_2}$, shown in Table 3, appreciably depend on the chosen values of k_u and k_m for the cases considered in Figure 3. A complete analysis of the influence of the coupling constants on the system properties will be addressed elsewhere.

4.3 Scale-dependence of the mesoscopic model

To conclude this section, we briefly consider the analysis of the system properties as a function of the degree of CGing, Φ. Although this issue will be examined more thoroughly elsewhere, let us introduce here a minimal model, satisfying the GenDPDE-M dynamics discussed in this manuscript, in which the scale factor $\Phi = 1$ and its number of mesoparticles N^0 is of the order of the total number of physical particles in the system, $\mathcal{N}^0$. Moreover, for the minimal model we have arbitrarily chosen a cutoff distance $R_{cut}^0 = 3$. Next, under the CGing process considered here, we group together $\Phi > 1$ particles into one coarser mesoparticle, so that the new number of mesoparticles is given by $N = N^0/\Phi$. However, we impose that the intensive variables, P, T and μ^α should remain invariant under this process. In addition, we also keep the total energy U and volume V unchanged, which implies that the system Helmholtz free energy F should remain invariant under this type of transformation. Notice that, in this decimation process, $c \equiv N^0/V = \Phi N/V$ is constant, by construction. Next, as a simple example, let us take the pressure of the system as approximately given by its mean field expression [13]
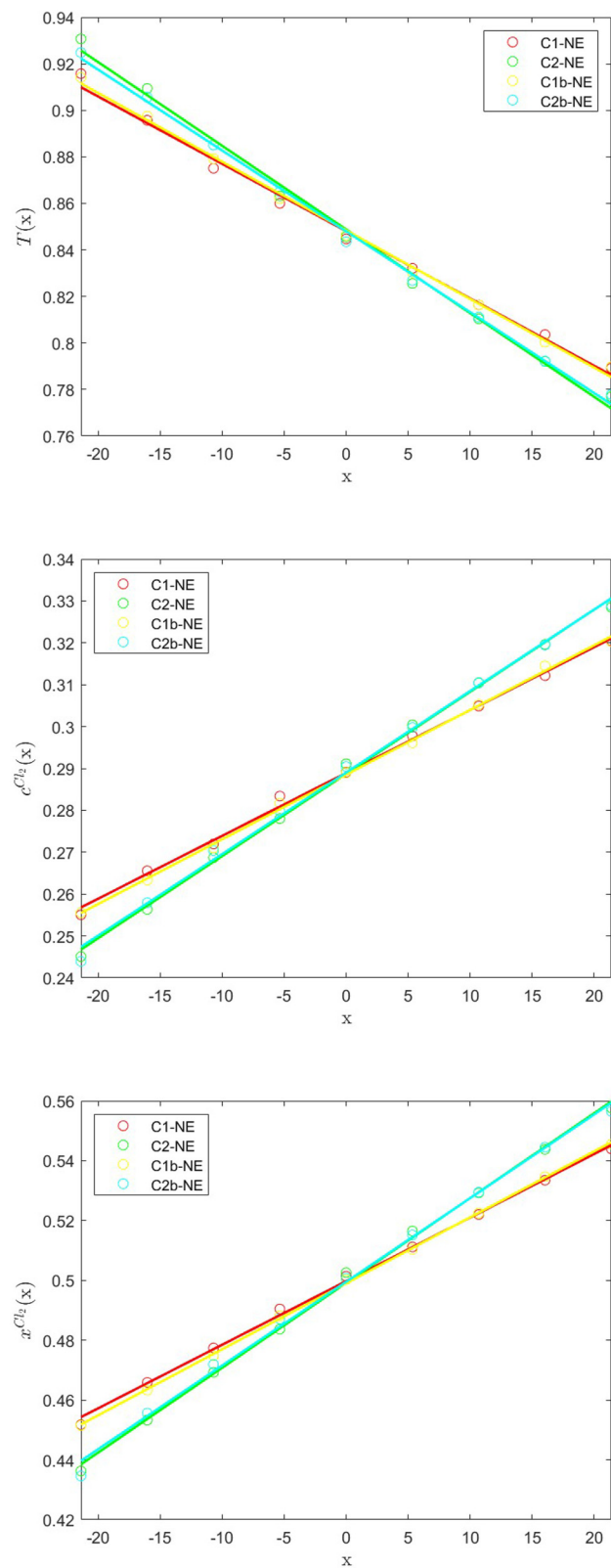
Figure 3: The *x*-profiles of the particle temperature (top), and the number concentration (middle) and molar fraction (bottom) of Cl_2 for the CG equimolar Ar/Cl_2 binary mixture at an initial temperature $T = 0.885$ and system number density $c = 0.577$, as obtained from the coupled GenDPDE-M simulations C1-NE and C2-NE and their analogous C1b-NE and C2b-NE. The circles represent simulation results, while the solid lines represent linear regressions. The results referring to identical sets of mesoscopic dynamic coefficients are in excellent agreement.

Table 3: Values of the thermal conductivity, λ, and the Soret coefficient for Cl_2, $s_T^{Cl_2}$, together with the heat flux density, J_x, the average temperature gradient, dT/dx, and the average molar fraction gradient of Cl_2, dx^{Cl_2}/dx, as obtained from non-equilibrium GenDPDE-M simulations.

| Test	$J_x \times 10^3$	$(dT/dx) \times 10^3$	$(dx^{Cl_2}/dx) \times 10^3$	λ	$s_T^{Cl_2}$
Dec-NE	6.46	-2.54 ± 0.05	1.67 ± 0.03	2.55 ± 0.05	2.64 ± 0.07
C1-NE	6.46	-2.89 ± 0.09	2.12 ± 0.04	2.23 ± 0.07	2.94 ± 0.10
C2-NE	6.46	-3.60 ± 0.10	2.84 ± 0.05	1.80 ± 0.05	3.15 ± 0.10
C3-NE	6.46	-3.12 ± 0.10	1.77 ± 0.06	2.07 ± 0.07	2.27 ± 0.11
C1b-NE	6.46	-2.95 ± 0.06	2.21 ± 0.02	2.19 ± 0.05	2.99 ± 0.07
C2b-NE	6.46	-3.47 ± 0.07	2.80 ± 0.06	1.86 ± 0.04	3.22 ± 0.10

$$P = k_B T n + \pi \zeta(\Phi) = k_B T \frac{c}{\Phi} + \pi \zeta(\Phi) \tag{100}$$

where $\zeta(\Phi)$ is proportional to the integration of the product of the weight function w with the pair distribution function g over the cutoff radius R_{cut}, $\zeta = \int d\mathbf{r} w(r) g(r)$. This parameter measures the local inhomogeneities in the particle distribution due to the presence of the interparticle pair potential interaction at the present degree of CGing. Hence, from Eq. (83), we can write Eq. (100) as

$$P = k_B T \frac{c}{\Phi}(1 - \zeta(\Phi)) + \pi^{EoS}(T, c) \zeta(\Phi) \tag{101}$$

In addition, we consider that $R_{cut}(\Phi) = \Phi^{1/3} R_{cut}^0$ to maintain the same number of neighbors within the interaction range, independently of Φ. It is important to realize that π^{EoS} is invariant under this type of transformation, as it depends only on c, according to Eqs. (83)–(85), and the fact that $n = c/\Phi$. We can thus conclude that Eq. (101) depends on the degree of CGing, and the invariance of P under the decimation transformation depends on how far $\zeta(\Phi)$ deviates from 1. The effect of such deviations at a given degree of CGing can be absorbed into the renormalization of the parameters of the model. Unfortunately, this analysis requires a separate treatment as $\zeta(\Phi)$ is a complex quantity that depends on the overall behavior of the system, notably on π^{EoS} itself as well as on the thermodynamic conditions of the system.

To numerically illustrate these facts, we have conducted simulations at different degrees of CGing. Figure 4 shows the variation of the system pressure P and the internal energy per particle $u = U/N^0$ as a function of Φ
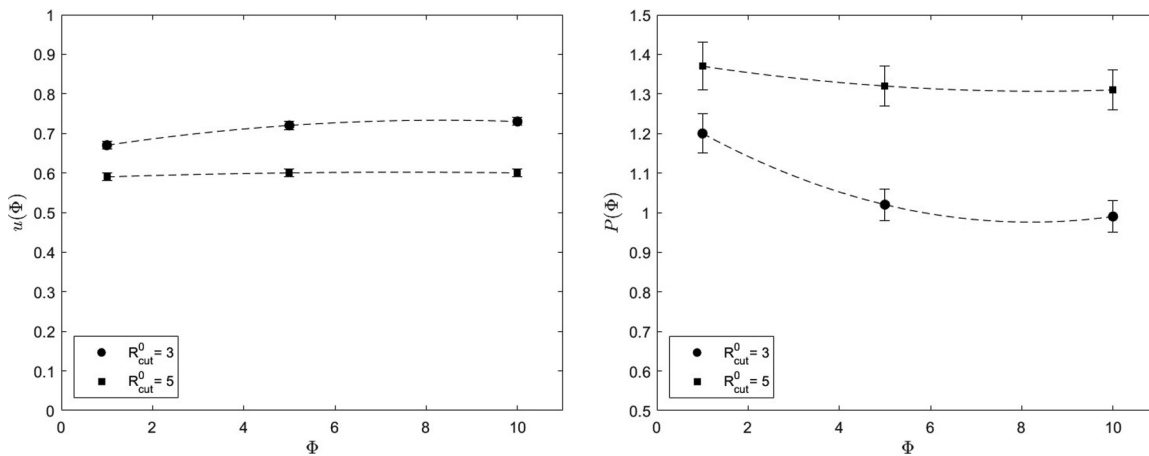
Figure 4: The system internal energy per physical particle (top) and the system pressure (bottom) as functions of the level of CGing, for an equimolar Ar/Cl_2 mixture at an initial temperature $T = 0.885$ and system number density $c = 0.5775$. The thermodynamic $u = 0.56$, and the thermodynamic $P = 1.44$.

for an equimolar Ar/Cl_2 mixture at a temperature $T = 0.885$ and number density $c = 0.5775$, as obtained from GenDPDE-M simulations. The figure also illustrates the effect of the number of neighbors, which depends on the chosen value of the cutoff radius. In our analysis, two different nominal cutoff radii were used, namely, $R_{cut}^0 = 3$ and 5. It can be observed that the scale invariance is attained if we increase the number of CG particles, but also if we increase the number of neighbors. The latter is an effect of the density-dependent potentials, as the fluctuations in the particle density Δn within R_{cut} decrease as $\Delta n \sim \sqrt{n/R_{cut}^3}$. Therefore, the scale-invariant mean field behavior observed at a higher degree of CGing and with a larger number of neighbors, is lost at a lower degree of CGing, which should be properly accounted for in the interparticle potential.

5 Conclusions

The Generalized Energy-Conserving Dissipative Particle Dynamics with Mass Transfer method (GenDPDE-M) was introduced in Refs. [24], [25] as an extension of the GenDPDE algorithm to simulate mesoparticles with variable composition. These original publications, being a proof of concept, only dealt with the particular case in which energy and mass transport between particles were dynamically decoupled. In real systems, however, it is well known that the energy fluxes entrain mass transport, and vice versa, leading to the Ludwig–Soret and Dufour effects [26]. In this article, we have developed the theoretical framework required to describe such coupled energy and material transport at the mesoscale. With this addition, GenDPDE-M can simulate general complex physicochemical scenarios in which the simultaneous transport of energy and matter takes place at the mesoscale; the method is therefore complete.

The extension presented in this article is formulated through the introduction of novel forms for the heat and diffusive fluxes between the mesoparticles. Here, these fluxes depend on both temperature and chemical potential differences, following Onsager's formulation of non-equilibrium thermodynamics. Since the GenDPDE-M method is formulated as Langevin-like equations, with random contributions simulating the effect of the hydrodynamic fluctuations [3], expressions for the amplitudes of these random terms need to be derived. Starting from Detailed Balance as the physical link between the mesoscopic model and the underlying physical system, we obtained the necessary Fluctuation-Dissipation theorems providing these amplitudes as functions of particle state variables, such as temperature, and also on the dynamic coefficients, which include the coupling. Interestingly, Detailed Balance is sufficient to also demonstrate that Onsager's reciprocal relations are valid at the mesoscale.

The consistency of the algorithm is demonstrated by showing that the simulated dynamics effectively samples the equilibrium probability distributions indicated in Eq. (67). We have checked that the distributions are independent of the values of the mesoscopic transport coefficients as well as the dynamic coupling between energy and mass. For completeness, a non-equilibrium simulation scheme, analogous to the setup of a real experiment, was conceived with the aim of reproducing the Ludwig–Soret effect for a specific two-component system. The mesoscopic thermodynamic model employed was the van der Waals one-fluid model describing an Ar/Cl_2 mixture. It is shown that GenDPDE-M not only properly reproduces this phenomenon, but crucially also allows us to control the strength of the Ludwig–Soret effect through the appropriate choice of the mesoscopic Onsager's cross-coefficient L_{ij}^{um}, coupling energy and material fluxes between particles i and j.

The framework developed in this article aims at the simulation of multicomponent systems, including moving interfaces, which are particularly relevant in areas such as chemical engineering, heat transport, materials engineering, among many others. The most natural step forward is to extend the algorithm to include chemical reactions within the mesoparticles, coupled to energy and matter transport, which will permit the simulation of reactive systems with moving interfaces, e.g., detonation and combustion, interfacial growth, among many other situations in which complex fluid processes may take place. Such an extension will be done elsewhere. Furthermore, the use of more complex EoS for the particle thermodynamic description, such as the Lennard–Jones [31], [39], Exponential-6 [40]–[42] or Statistical Associated Fluid Theory [43] EoS, enables the application of the method to a panoply of different materials and processes.

Appendix A: Alternative formulation of the heat and diffusive fluxes

With the purpose of exploring the possible definition of alternative expressions for the heat and diffusive fluxes, defined in Eqs. (34) and (35), let us introduce the following definitions:

$$\frac{1}{\mathcal{T}} \equiv \frac{1}{2}\left(\frac{1}{\bar{\theta}_i} + \frac{1}{\bar{\theta}_j}\right) \tag{A1}$$

$$\mathcal{M} \equiv \frac{1}{2}\left(\bar{\bar{\mu}}_i + \bar{\bar{\mu}}_j\right) \tag{A2}$$

$$\Delta\frac{1}{\bar{\theta}} \equiv \frac{1}{2}\left(\frac{1}{\bar{\theta}_i} - \frac{1}{\bar{\theta}_j}\right) \tag{A3}$$

$$\Delta\bar{\bar{\mu}} \equiv \frac{1}{2}\left(\bar{\bar{\mu}}_i - \bar{\bar{\mu}}_j\right) \tag{A4}$$

In view of these equations, the condition $\dot{\mathcal{F}} < 0$ in Eq. (31) can be rewritten as

$$\left\{T\left(-2\Delta\frac{1}{\bar{\theta}}\right)\dot{q}_{ij} + T\left[(\mathcal{M}+\Delta\bar{\mu})\left(\frac{1}{\mathcal{T}}+\Delta\frac{1}{\bar{\theta}}\right) - (\mathcal{M}-\Delta\bar{\mu})\left(\frac{1}{\mathcal{T}}-\Delta\frac{1}{\bar{\theta}}\right)\right]J_{ij}^{A}\right\} < 0 \tag{A5}$$

After some algebra, Eq. (A5) becomes

$$\left[-2\Delta\frac{1}{\bar{\theta}}\dot{q}_{ij} + \left(2\mathcal{M}\Delta\frac{1}{\bar{\theta}} + 2\frac{1}{\mathcal{T}}\Delta\bar{\bar{\mu}}\right)J_{ij}^{A}\right] < 0 \tag{A6}$$

We recall that the bare chemical potential is a function of the bare temperature, according to Eqs. (94) and (95). Hence, the quantities $\mathcal{M}$ and $\Delta\bar{\bar{\mu}}$ are functions of the particle bare temperature as well and, therefore, an expansion around the *central temperature* $\mathcal{T}$ can be invoked. It is thus possible to express the term $\mathcal{M}$ in Eq. (A6) as

$$\mathcal{M} \simeq \mathcal{M}|_{\mathcal{T}} + \frac{1}{2}\left[\frac{\partial\bar{\bar{\mu}}_i}{\partial\frac{1}{\bar{\theta}_i}}\bigg|_{\mathcal{T}}\Delta\frac{1}{\bar{\theta}} - \frac{\partial\bar{\bar{\mu}}_j}{\partial\frac{1}{\bar{\theta}_j}}\bigg|_{\mathcal{T}}\Delta\frac{1}{\bar{\theta}}\right] + \mathcal{O}(\Delta)^2$$

$$\simeq \mathcal{M}|_{\mathcal{T}} - \mathcal{T}^2\frac{1}{2}\left(\frac{\partial\bar{\bar{\mu}}_i}{\partial\bar{\theta}_i}\bigg|_{\mathcal{T}} - \frac{\partial\bar{\bar{\mu}}_j}{\partial\bar{\theta}_j}\bigg|_{\mathcal{T}}\right)\Delta\frac{1}{\bar{\theta}} + \mathcal{O}\left(\Delta\frac{1}{\bar{\theta}}\right)^2 \simeq \mathcal{M}|_{\mathcal{T}} + \mathcal{O}(\Delta)^2 \tag{A7}$$

where $\mathcal{O}(\Delta)^2$ here represents general second order differences in particle properties. Here, the subscript $\mathcal{T}$ indicates that the function should be evaluated at $\mathcal{T}$ rather than at the actual particle bare temperature $\tilde{\theta}$. Moreover, the term $2\Delta\bar{\bar{\mu}}$ in Eq. (A6) can be written as,

$$2\Delta\bar{\bar{\mu}} = \bar{\bar{\mu}}_i\left(\frac{1}{\bar{\theta}_i}\right) - \bar{\bar{\mu}}_j\left(\frac{1}{\bar{\theta}_j}\right)$$

$$= \left[\bar{\bar{\mu}}_i\left(\frac{1}{\mathcal{T}}\right) - \bar{\bar{\mu}}_j\left(\frac{1}{\mathcal{T}}\right)\right] + \left[\bar{\bar{\mu}}_i\left(\frac{1}{\bar{\theta}_i}\right) - \bar{\bar{\mu}}_i\left(\frac{1}{\mathcal{T}}\right) - \bar{\bar{\mu}}_j\left(\frac{1}{\bar{\theta}_j}\right) + \bar{\bar{\mu}}_j\left(\frac{1}{\mathcal{T}}\right)\right]$$

$$\simeq 2\Delta\bar{\bar{\mu}}|_{\mathcal{T}} + \left(\frac{\partial\bar{\bar{\mu}}_i}{\partial\frac{1}{\bar{\theta}_i}}\bigg|_{\mathcal{T}}\Delta\frac{1}{\bar{\theta}} + \frac{\partial\bar{\bar{\mu}}_j}{\partial\frac{1}{\bar{\theta}_j}}\bigg|_{\mathcal{T}}\Delta\frac{1}{\bar{\theta}}\right)$$

$$= 2\Delta\bar{\bar{\mu}}|_{\mathcal{T}} - \mathcal{T}^2\left(\frac{\partial\bar{\bar{\mu}}_i}{\partial\tilde{\theta}_i}\bigg|_{\mathcal{T}} + \frac{\partial\bar{\bar{\mu}}_j}{\partial\tilde{\theta}_j}\bigg|_{\mathcal{T}}\right)\Delta\frac{1}{\bar{\theta}} + \mathcal{O}\left(\Delta\frac{1}{\bar{\theta}}\right)^2 \tag{A8}$$

According to our formulation of the particle dynamics, the mass and energy transfer occur at constant local density, as the kinematic move takes place separately from thermodynamic property exchange moves. Hence, we must consider that the transfer occurs at constant volume (or local density n). Therefore, rather than proceeding by introducing $\partial\mu/\partial\theta|_\pi = -s$, as is usually done, we have instead $\partial\mu/\partial\theta|_n = -s - (n/\kappa_T)\partial\mu/\partial\pi|_\theta$, as the processes are not at constant pressure.

At this point, it is rather obvious that the analogy with the macroscopic definition of the measurable heat flux cannot be continued further. From one perspective, the expansion of the thermodynamic properties around the central temperature precludes the possibility of having large particle temperature differences, which may be present in some situations of interest for the application of our model. Notice that, even in equilibrium, the temperature differences between particles are of the order of $\Delta(1/\theta) \sim (\sqrt{k_B/C_V})/T$, which may be not negligible if the particle heat capacity $C_V \sim k_B$. From another perspective, even if the linearization approximation holds, the function $S|_{\mathcal{T}}$, defined as,

$$S|_{\mathcal{T}} \equiv -\frac{1}{2}\left(\frac{\partial\bar{\bar{\mu}}_i}{\partial\tilde{\theta}_i}\bigg|_{\mathcal{T}} + \frac{\partial\bar{\bar{\mu}}_j}{\partial\tilde{\theta}_j}\bigg|_{\mathcal{T}}\right) \neq \frac{1}{2}\left(\tilde{s}_i|_{\mathcal{T}} + \tilde{s}_j|_{\mathcal{T}}\right) \tag{A9}$$

cannot be related to the particle entropies, as $\frac{\partial\bar{\bar{\mu}}_i}{\partial\tilde{\theta}_i}\big|_{\mathcal{T}} \neq \tilde{s}_i|_{\mathcal{T}}$. For the sake of completeness, let us introduce $S|_{\mathcal{T}}$, as defined in Eqs. (A9), into (A6). Therefore, the condition $\dot{\tilde{\mathcal{F}}} < 0$ becomes,

$$\left[-2\Delta\frac{1}{\bar{\theta}}\dot{q}_{ij} + \left(2\mathcal{M}|_{\mathcal{T}}\Delta\frac{1}{\bar{\theta}} + 2\frac{1}{\mathcal{T}}\Delta\bar{\bar{\mu}}|_{\mathcal{T}} + 2\mathcal{T}S|_{\mathcal{T}}\Delta\frac{1}{\bar{\theta}}\right)J_{ij}^{\mathrm{A}}\right] < 0 \tag{A10}$$

where again we have retained terms up to the first order only. Further, manipulating Eq. (A10) by introducing

$$\mathcal{H}|_{\mathcal{T}} \equiv \mathcal{M}|_{\mathcal{T}} + \mathcal{T}S|_{\mathcal{T}} \tag{A11}$$

we can write,

$$\left[-2\Delta\frac{1}{\bar{\theta}}\dot{q}_{ij} + \left(2\mathcal{M}|_{\mathcal{T}}\Delta\frac{1}{\bar{\theta}} + 2\frac{1}{\mathcal{T}}\Delta\bar{\bar{\mu}}|_{\mathcal{T}} + 2\mathcal{T}S|_{\mathcal{T}}\Delta\frac{1}{\bar{\theta}}\right)J_{ij}^{\mathrm{A}}\right]$$

$$= \left[-2\Delta\frac{1}{\bar{\theta}}\dot{q}_{ij} + \left(2(\mathcal{M}|_{\mathcal{T}} + \mathcal{T}S|_{\mathcal{T}})\Delta\frac{1}{\bar{\theta}} + 2\frac{1}{\mathcal{T}}\Delta\bar{\bar{\mu}}|_{\mathcal{T}}\right)J_{ij}^{\mathrm{A}}\right]$$

$$
\begin{aligned}
&= \left[-2\Delta \frac{1}{\bar{\theta}} \dot{q}_{ij} + \left(2\mathcal{H}|_{\mathcal{T}} \Delta \frac{1}{\bar{\theta}} + 2\frac{1}{\mathcal{T}} \Delta \bar{\mu}|_{\mathcal{T}} \right) J_{ij}^{\mathrm{A}} \right] \\
&= \left[-2 \left(\dot{q}_{ij} - \mathcal{H}|_{\mathcal{T}} J_{ij}^{\mathrm{A}} \right) \Delta \frac{1}{\bar{\theta}} + 2\frac{1}{\mathcal{T}} \Delta \bar{\mu}|_{\mathcal{T}} J_{ij}^{\mathrm{A}} \right] \\
&= \left[-2 \dot{q}_{ij}' \Delta \frac{1}{\bar{\theta}} + 2\frac{1}{\mathcal{T}} \Delta \bar{\mu}|_{\mathcal{T}} J_{ij}^{\mathrm{A}} \right] < 0
\end{aligned}
\tag{A12}
$$

where we have defined what would be the analogous expression of the measurable heat flux at the mesoscale, i.e.,

$$
\dot{q}_{ij}' \equiv \dot{q}_{ij} - \mathcal{H}|_{\mathcal{T}} J_{ij}^{\mathrm{A}}
\tag{A13}
$$

Although we show that, under specific thermodynamic conditions the measurable heat flux can be defined, we stress that the quantity $\mathcal{S}$ cannot be interpreted as any given form of particle entropy, in view of Eq. (A9). As a consequence, $\mathcal{H}$ cannot be calculated in terms of particle enthalpies, which are forcibly defined as $h = \mu + \theta s$, either. All in all, using this transformation at the mesoscopic level results in the loss of any intuitive benefit.

Appendix B: Fluctuation-Dissipation theorem

The relation between the matrices containing the mesoscopic transport coefficients, $\mathbf{L}_{ij}$, and the amplitudes of the random terms, $\boldsymbol{\sigma}_{ij}$, as defined in Eq. (48) follows from the evaluation of the second moment of the system distribution [11], [12] and use of DB. We remind the reader that the validity of DB is only based on the form of the Hamiltonian of the underlying microscopic physical system, together with the time-reversibility of the trajectories of the latter [44]. Therefore, as GenDPDE-M aims at simulating physical systems, the assumption of DB is the most basic assumption that connects its structure to the physical nature of the processes of the system.

Thus, the second moment of the fluctuating mesoscopic state vector $\mathbf{x}_i$, defined in Eq. (47) is given by

$$
\langle \mathbf{x}_i \mathbf{x}_i^T \rangle = \int \mathrm{d}\tilde{\Gamma} \mathrm{d}\tilde{\Gamma}' P_{\mathrm{eq}}(\tilde{\Gamma}) \mathbf{x}_i' \mathbf{x}_i'^T W(\tilde{\Gamma} \to \tilde{\Gamma}') \delta t
\tag{B1}
$$

where $W(\tilde{\Gamma} \to \tilde{\Gamma}')$ represents the transition probability per unit time with the property

$$
\int \mathrm{d}\tilde{\Gamma}' W(\tilde{\Gamma} \to \tilde{\Gamma}') \delta t = 1
\tag{B2}
$$

due to causality. Here, $\tilde{\Gamma}$ represents the full state of the mesoparticles, i.e., $\tilde{\Gamma} \equiv (\mathbf{x}_1, \mathbf{x}_2, \dots, \mathbf{x}_N)$. The tilde indicates that we are using bare variables to define the state of the system. By construction, the random terms are not correlated with any other variables at the same instant of time. Then, using the compact EoM Eq. (46) to evaluate $\mathbf{x}_i' \mathbf{x}_i'^T$ and retaining terms up to order O (δt) only, we obtain

$$
\mathbf{x}_i' \mathbf{x}_i'^T = \mathbf{x}_i \mathbf{x}_i^T + \mathbf{x}_i (\mathbf{L}_{ij} \cdot \mathbf{Y}_{ij})^T \delta t + (\mathbf{L}_{ij} \cdot \mathbf{Y}_{ij}) \mathbf{x}_i^T \delta t + (\boldsymbol{\sigma}_{ij} \cdot \boldsymbol{\Omega}_{ij})(\boldsymbol{\sigma}_{ij} \cdot \boldsymbol{\Omega}_{ij})^T \delta t
$$

Here, we have only considered a given pair of mesoparticles i and j as the FD theorem has to be satisfied by any given number of pairs, which ultimately implies it should be satisfied individually for every pair. In view of this, we have restricted our demonstration to a given pair for simplicity of notation and clarity, but with no loss of generality. Hence,

$$
\langle \mathbf{x}_i \mathbf{x}_i^T \rangle = \int \mathrm{d}\tilde{\Gamma} P_{eq}(\tilde{\Gamma}) \left[\mathbf{x}_i \mathbf{x}_i^T + \mathbf{x}_i (\mathbf{L}_{ij} \cdot \mathbf{Y}_{ij})^T \delta t + (\mathbf{L}_{ij} \cdot \mathbf{Y}_{ij}) \mathbf{x}_i^T \delta t + \langle (\boldsymbol{\sigma}_{ij} \cdot \boldsymbol{\Omega}_{ij})(\boldsymbol{\sigma}_{ij} \cdot \boldsymbol{\Omega}_{ij})^T \rangle_{\boldsymbol{\Omega}} \delta t \right]
\tag{B3}
$$

Note that the first term on the right-hand side of Eq. (B3) is exactly $\langle \mathbf{x}_i \mathbf{x}_i^T \rangle$, which cancels the left-hand side. Then, using the properties of the transposed matrix, we get

$$
0 = \int \mathrm{d}\tilde{\Gamma} P_{\mathrm{eq}}(\tilde{\Gamma}) \left\{ \left[(\mathbf{L}_{ij} \cdot \mathbf{Y}_{ij}) \mathbf{x}_i^T \right]^T + (\mathbf{L}_{ij} \cdot \mathbf{Y}_{ij}) \mathbf{x}_i^T + \langle (\boldsymbol{\sigma}_{ij} \cdot \boldsymbol{\Omega}_{ij})(\boldsymbol{\sigma}_{ij} \cdot \boldsymbol{\Omega}_{ij})^T \rangle_{\boldsymbol{\Omega}} \right\}
\tag{B4}
$$

Next, let us focus on individual terms on the right-hand side of Eq. (B4) separately. We start with rewriting the second term as

$$
\int d\tilde{\Gamma} P_{\mathrm{eq}}(\tilde{\Gamma})(\mathbf{L}_{ij} \cdot \mathbf{Y}_{ij})\mathbf{x}_i^T
$$

$$
= \int d\tilde{\Gamma} \mathbf{L}_{ij} \left(P_{\mathrm{eq}}(\tilde{\Gamma}) \mathbf{Y}_{ij} \mathbf{x}_i^T \right)
$$

$$
= \int d\tilde{\Gamma} \mathbf{L}_{ij} \left[k_B \left(\frac{\partial P_{\mathrm{eq}}}{\partial \mathbf{x}_i} - \frac{\partial P_{\mathrm{eq}}}{\partial \mathbf{x}_j} \right) \mathbf{x}_i^T \right]
$$

$$
= - \int d\tilde{\Gamma} P_{\mathrm{eq}}(\tilde{\Gamma}) k_B \mathbf{L}_{ij} \tag{B5}
$$

where partial integration and independence of $\mathbf{L}_{ij}$ from u_i and m_i^A (the EoM Eq. (46) are linear in Onsager's sense) have been used to arrive to the last equality. The first term is simply the transpose of the second term, i.e.,

$$
\int d\tilde{\Gamma} P_{\mathrm{eq}}(\tilde{\Gamma}) \left[(\mathbf{L}_{ij} \cdot \mathbf{Y}_{ij})\mathbf{x}_i^T \right]^T = - \int d\tilde{\Gamma} P_{\mathrm{eq}}(\tilde{\Gamma}) k_B \mathbf{L}_{ij}^T \tag{B6}
$$

Finally, the third term can be rewritten as

$$
\int d\tilde{\Gamma} P_{\mathrm{eq}}(\tilde{\Gamma}) \langle (\boldsymbol{\sigma}_{ij} \cdot \boldsymbol{\Omega}_{ij})(\boldsymbol{\sigma}_{ij} \cdot \boldsymbol{\Omega}_{ij})^T \rangle_{\boldsymbol{\Omega}}
$$

$$
= \int d\tilde{\Gamma} P_{\mathrm{eq}}(\tilde{\Gamma}) \langle (\boldsymbol{\sigma}_{ij} \cdot \boldsymbol{\Omega}_{ij}) \left(\boldsymbol{\Omega}_{ij}^T \boldsymbol{\sigma}_{ij}^T \right) \rangle_{\boldsymbol{\Omega}}
$$

$$
= \int d\tilde{\Gamma} P_{\mathrm{eq}}(\tilde{\Gamma}) \boldsymbol{\sigma}_{ij} \langle \boldsymbol{\Omega}_{ij} \boldsymbol{\Omega}_{ij}^T \rangle_{\boldsymbol{\Omega}} \boldsymbol{\sigma}_{ij}^T
$$

$$
= \int d\tilde{\Gamma} P_{\mathrm{eq}}(\tilde{\Gamma}) \boldsymbol{\sigma}_{ij} \cdot \boldsymbol{\sigma}_{ij}^T \tag{B7}
$$

where use has been made of the properties of the normalized random numbers, Eqs. (43) and (44), together with Eq. (47). Inserting Eqs. (B5)–(B7) into (B4), we get

$$
0 = \int d\tilde{\Gamma} P_{\mathrm{eq}}(\tilde{\Gamma}) \left[-k_B \left(\mathbf{L}_{ij} + \mathbf{L}_{ij}^T \right) + \boldsymbol{\sigma}_{ij} \cdot \boldsymbol{\sigma}_{ij}^T \right] \tag{B8}
$$

As we demand that the dynamic coefficients of the model be independent of the reservoir characteristics contained in $P_{\mathrm{eq}}(\tilde{\Gamma})$, to satisfy Eq. (B8) we further impose that

$$
\boldsymbol{\sigma}_{ij} \cdot \boldsymbol{\sigma}_{ij}^T = k_B \left(\mathbf{L}_{ij} + \mathbf{L}_{ij}^T \right) \tag{B9}
$$

Equation (B9) represents the general FD theorem relating the mesoscopic transport coefficients to the amplitudes of the thermal fluctuations.

Appendix C: Onsager's reciprocal relations

Demonstration of Onsager's reciprocal relations for the mesoscopic transport coefficients follows from the evaluation of the autocorrelation of the state vectors at different times, i.e.,

$$
\langle \mathbf{x}_i \mathbf{x}_i'^T \rangle = \int d\tilde{\Gamma} d\tilde{\Gamma}' P_{\mathrm{eq}}(\tilde{\Gamma}) W(\tilde{\Gamma} \rightarrow \tilde{\Gamma}') \delta t \, \mathbf{x}_i \mathbf{x}_i'^T \tag{C1}
$$

Using the compact form of the EoM Eq. (46), together with the property of the transition probability Eq. (B2) and the fact that the random terms are not correlated to other state variables at the same instant of time, we can rewrite Eq. (C1) as

$$\langle \mathbf{x}_i \mathbf{x}_i'^T \rangle = \int \mathrm{d}\tilde{\Gamma} P_{\text{eq}}(\tilde{\Gamma}) \big[\mathbf{x}_i \mathbf{x}_i^T + \mathbf{x}_i (\mathbf{L}_{ij} \cdot \mathbf{Y}_{ij})^T \delta t \big] \tag{C2}$$

Analogously to Appendix B, in this demonstration we only consider a pair of mesoparticles, namely i and j, as the validity of ORR should be independent of the number of pairs. Next, using DB [44],

$$P_{\text{eq}}(\tilde{\Gamma}) W(\tilde{\Gamma} \to \tilde{\Gamma}') \delta t = P_{\text{eq}}(\tilde{\Gamma}^*) W(\tilde{\Gamma}^* \to \tilde{\Gamma}^{*\prime}) \delta t$$

it follows that

$$\begin{aligned} \langle \mathbf{x}_i \mathbf{x}_i'^T \rangle &= \int \mathrm{d}\tilde{\Gamma} \mathrm{d}\tilde{\Gamma}' P_{\text{eq}}(\tilde{\Gamma}) W(\tilde{\Gamma} \to \tilde{\Gamma}') \, \delta t \, \mathbf{x}_i \mathbf{x}_i'^T \\ &= \int \mathrm{d}\tilde{\Gamma} \mathrm{d}\tilde{\Gamma}' P_{\text{eq}}(\tilde{\Gamma}^*) W(\tilde{\Gamma}^* \to \tilde{\Gamma}^{*\prime}) \delta t \, \mathbf{x}_i \mathbf{x}_i'^T \\ &= \int \mathrm{d}\tilde{\Gamma}^* \mathrm{d}\tilde{\Gamma}^{*\prime} P_{\text{eq}}(\tilde{\Gamma}^*) W(\tilde{\Gamma}^* \to \tilde{\Gamma}^{*\prime}) \, \delta t \, \mathbf{x}_i^{*\prime} \mathbf{x}_i^{*T} \\ &= \langle \mathbf{x}_i' \mathbf{x}_i^T \rangle \end{aligned}$$

where

$$\langle \mathbf{x}_i' \mathbf{x}_i^T \rangle = \int \mathrm{d}\tilde{\Gamma} P_{\text{eq}}(\tilde{\Gamma}) \big[\mathbf{x}_i \mathbf{x}_i^T + (\mathbf{L}_{ij} \cdot \mathbf{Y}_{ij}) \mathbf{x}_i^T \delta t \big] \tag{C3}$$

Equating the right-hand sides of Eqs. (C2) and (C3), and using the properties of the transposed matrix, we get

$$\int \mathrm{d}\tilde{\Gamma} P_{\text{eq}}(\tilde{\Gamma}) \big[(\mathbf{L}_{ij} \cdot \mathbf{Y}_{ij}) \mathbf{x}_i^T \big]^T = \int \mathrm{d}\tilde{\Gamma} P_{\text{eq}}(\tilde{\Gamma}) (\mathbf{L}_{ij} \cdot \mathbf{Y}_{ij}) \mathbf{x}_i^T \tag{C4}$$

The above integrals were already solved in Eqs. (B5) and (B6). Invoking again the independence of $\mathbf{L}_{ij}$ from the reservoir properties, Eq. (C4) is satisfied if we further demand that

$$\mathbf{L}_{ij} = \mathbf{L}_{ij}^T \tag{C5}$$

Therefore, we conclude that, for a binary mixture, the condition $L_{ij}^{um} = L_{ij}^{mu}$ corresponds to the sought ORR for the system at the mesoscopic level and for every pair of particles.

References

[1] P. J. Hoogerbrugge and J. M. V. A. Koelman, "Simulating microscopic hydrodynamic phenomena with dissipative particle dynamics," *Europhys. Lett.*, vol. 19, no. 3, pp. 155–160, 1992.

[2] J.-P. Hansen and I. R. McDonald, *Theory of Simple Liquids*, Oxford, Elsevier, 2006.

[3] L. D. Landau and E. M. Lifshitz, *Fluid Mechanics. Landau and Lifshitz: Course of Theoretical Physics*, vol. 6, 2nd ed Oxford, Pergamon, 1987.

[4] P. Español and P. B. Warren, "Statistical mechanics of dissipative particle dynamics," *Europhys. Lett.*, vol. 30, no. 4, pp. 191–196, 1995.

[5] J. B. Avalos and A. D. Mackie, "Dissipative particle dynamics with energy conservation," *Europhys. Lett.*, vol. 40, no. 2, pp. 141–146, 1997.

[6] P. Español, "Dissipative particle dynamics with energy conservation," *Europhys. Lett.*, vol. 40, no. 6, pp. 631–636, 1997.

[7] R. Qiao and P. He, "Simulation of heat conduction in nanocomposite using energy-conserving dissipative particle dynamics," *Mol. Simul.*, vol. 33, no. 8, pp. 677–683, 2007.

[8] G. C. Ganzenmüller, S. Hiermaier, and M. O. Steinhauser, "Shock-wave induced damage in lipid bilayers: a dissipative particle dynamics simulation study," *Soft Matter*, vol. 7, no. 9, pp. 4307–4317, 2011.

[9] Z. Li, Y.-H. Tang, X. Li, and G. E. Karniadakis, "Mesoscale modeling of phase transition dynamics of thermoresponsive polymers," *Chem. Commun.*, vol. 51, no. 55, pp. 11038–11040, 2015.

[10] E. O. Johansson, T. Yamada, B. Sundén, and J. Yuan, "Modeling mesoscopic solidification using dissipative particle dynamics," *Int. J. Therm. Sci.*, vol. 101, pp. 207−216, 2016.

[11] J. Bonet Avalos, M. Lísal, J. P. Larentzos, A. D. Mackie, and J. K. Brennan, "Generalised dissipative particle dynamics with energy conservation: density- and temperature-dependent potentials," *Phys. Chem. Chem. Phys.*, vol. 21, no. 45, pp. 24891−24911, 2019.

[12] J. Bonet Avalos, M. Lísal, J. P. Larentzos, A. D. Mackie, and J. K. Brennan, "Generalised dissipative particle dynamics with energy conservation revisited: insight from the thermodynamics of the mesoparticle leading to an alternative heat flow model," *Phys. Rev. E*, vol. 103, no. 6, p. 062128, 2021.

[13] I. Pagonabarraga and D. Frenkel, "Dissipative particle dynamics for interacting systems," *J. Chem. Phys.*, vol. 115, no. 11, pp. 5015−5026, 2001.

[14] P. B. Warren, "Vapor-liquid coexistence in many-body dissipative particle dynamics," *Phys. Rev. E*, vol. 68, no. 6, p. 066702, 2003.

[15] E. Moeendarbary, T. Y. Ng, and M. Zangeneh, "Dissipative particle dynamics: introduction, methodology and complex fluid applications — a review," *Int. J. Appl. Mech.*, vol. 1, no. 4, pp. 737−763, 2009.

[16] J. K. Brennan, M. Lísal, J. D. Moore, S. Izvekov, I. V. Schweigert, and J. P. Larentzos, "Coarse-grain model simulations of nonequilibrium dynamics in heterogeneous materials," *J. Phys. Chem. Lett.*, vol. 5, no. 12, pp. 2144−2149, 2014.

[17] J. D. Moore, *et al*, "A coarse-grain force field for RDX: density dependent and energy conserving," *J. Chem. Phys.*, vol. 144, no. 10, p. 104501, 2016.

[18] P. Español and P. B. Warren, "Perspective: dissipative particle dynamics," *J. Chem. Phys.*, vol. 146, no. 15, p. 150901, 2017.

[19] J. P. Larentzos, J. M. Mansell, M. Lísal, and J. K. Brennan, "Coarse-grain modelling using an equation-of-state many-body potential: application to fluid mixtures at high temperature and high pressure," *Mol. Phys.*, vol. 116, no. 21−22, pp. 3271−3282, 2018.

[20] K. P. Santo and A. V. Neimark, "Dissipative particle dynamics simulations in colloid and interface science: a review," *Adv. Colloid Interface Sci.*, vol. 298, p. 102545, 2021.

[21] Z. Li, Y.-H. Tang, H. Lei, B. Caswell, and G. E. Karniadakis, "Energy-conserving dissipative particle dynamics with temperature-dependent properties," *J. Comput. Phys.*, vol. 265, pp. 113−127, 2014.

[22] M. Lísal, J. P. Larentzos, J. B. Avalos, A. D. Mackie, and J. K. Brennan, "Generalized energy-conserving dissipative particle dynamics with reactions," *J. Chem. Theory Comput.*, vol. 18, no. 4, pp. 2503−2512, 2022.

[23] B. H. Lee, M. N. Sakano, J. P. Larentzos, J. K. Brennan, and A. Strachan, "A coarse-grain reactive model of RDX: molecular resolution at the μm scale," *J. Chem. Phys.*, vol. 158, no. 2, p. 024702, 2023.

[24] J. B. Avalos, M. Lísal, J. P. Larentzos, A. D. Mackie, and J. K. Brennan, "Generalized energy-conserving dissipative particle dynamics with mass transfer. Part 1: theoretical foundation and algorithm," *J. Chem. Theory Comput.*, vol. 18, no. 12, pp. 7639−7652, 2022.

[25] M. Lísal, J. B. Avalos, J. P. Larentzos, A. D. Mackie, and J. K. Brennan, "Generalized energy-conserving dissipative particle dynamics with mass transfer. Part 2: applications and demonstrations," *J. Chem. Theory Comput.*, vol. 18, no. 12, pp. 7653−7670, 2022.

[26] S. R. de Groot and P. Mazur, *Non-Equilibrium Thermodynamics*, New York, Dover Publications, INC., 1984.

[27] R. Taylor and R. Krishna, *Multicomponent Mass Transfer*, New York, Wiley, 1993.

[28] L. Onsager and S. Machlup, "Fluctuations and irreversible processes," *Phys. Rev.*, vol. 91, no. 6, pp. 1505−1512, 1953.

[29] H. B. Callen, *Thermodynamics and an Introduction to Thermostatistics*, New York, John Wiley & Sons, 1985.

[30] J. Armstrong and F. Bresme, "Thermal conductivity of highly asymmetric binary mixtures: how important are heat/mass coupling effects?," *Phys. Chem. Chem. Phys.*, vol. 16, no. 24, pp. 12307−12316, 2014.

[31] J. K. Johnson, J. A. Zollweg, and K. E. Gubbins, "The Lennard-Jones equation of state revisited," *Mol. Phys.*, vol. 78, no. 3, pp. 591−618, 1993.

[32] J. R. Elliott and T. C. Lira, *Introductory Chemical Engineering Thermodynamics*, New York, Prentice Hall, 2012.

[33] T. Y. Kwak and G. A. Mansoori, "Van der Waals mixing rules for cubic equations of state. applications for supercritical fluid extraction modelling," *Chem. Eng. Sci.*, vol. 41, no. 5, pp. 1303−1309, 1986.

[34] M. Lísal, J. K. Brennan, and J. B. Avalos, "Dissipative particle dynamics at isothermal, isobaric, isoenergetic, and isoenthalpic conditions using Shardlow-like splitting algorithms," *J. Chem. Phys.*, vol. 135, no. 20, p. 204105, 2011.

[35] J. P. Larentzos, J. K. Brennan, J. D. Moore, M. Lísal, and W. D. Mattson, "Parallel implementation of isothermal and isoenergetic dissipative particle dynamics using Shardlow-like splitting algorithms," *Comput. Phys. Commun.*, vol. 185, no. 7, pp. 1987−1998, 2014.

[36] L. B. Lucy, "A numerical approach to the testing of the fission hypothesis," *Astron. J.*, vol. 82, pp. 1013−1024, 1977.

[37] F. Müller-Plathe and P. Bordat, "Reverse non-equilibrium molecular dynamics," *Lect. Notes Phys.*, vol. 640, pp. 310−326, 2004.

[38] C. Nieto-Draghi and J. B. Avalos, "Non-equilibrium momentum exchange algorithm for molecular dynamics simulation of heat flow in multicomponent systems," *Mol. Phys.*, vol. 101, no. 14, pp. 2303−2307, 2003.

[39] J. Kolafa and I. Nezbeda, "The Lennard-Jones fluid: an accurate analytic and theoretically-based equation of state," *Fluid Phase Equil.*, vol. 100, pp. 1−34, 1994.

[40] H. Vörtler, I. Nezbeda, and M. Lísal, "The exp-6 potential fluid at very high pressures: computer simulations and theory," *Mol. Phys.*, vol. 92, no. 5, pp. 813−824, 1997.

[41] M. Lísal, W. R. Smith, and I. Nezbeda, "Computer simulation of the thermodynamic properties of high-temperature chemically-reacting plasmas," *J. Chem. Phys.*, vol. 113, no. 12, pp. 4885−4895, 2000.

[42] J.-X. Sun, Q. Wu, L. Cai, and F. Jing, "Analytic equation of state for exponential-six fluid based on the ross variational perturbation theory and the Percus—Yevick radial distribution function of hard spheres," *Chem. Phys. Lett.*, vol. 449, no. 1, pp. 72—76, 2007.

[43] W. G. Chapman, K. E. Gubbins, G. Jackson, and M. Radosz, "New reference equation of state for associating liquids," *Ind. Eng. Chem. Res.*, vol. 29, no. 8, pp. 1709—1721, 1990.

[44] N. G. van Kampen, *Stochastic Processes in Physics and Chemistry*, Amsterdam, North Holland, 1992.